

# ***METTL3-mediated m<sup>6</sup>A modification regulates CDKN1A to attenuate chronic sleep deprivation-induced cognitive impairment and neuronal apoptosis in rats***

---

Received: 16 August 2025

---

Revised: 17 December 2025

---

Accepted: 24 January 2026

---

Cite this article as: Xing, F., Shi, X.-S., Gu, H.-W. et al. *METTL3-mediated m<sup>6</sup>A modification regulates CDKN1A to attenuate chronic sleep deprivation-induced cognitive impairment and neuronal apoptosis in rats*. *Transl Psychiatry* (2026). <https://doi.org/10.1038/s41398-026-03855-4>

Fei Xing, Xiao-Shan Shi, Han-Wen Gu, Pan-Miao Liu, Lei Lei, Min Jia, Xing-Ming Wang, Mu-Huo Ji & Jian-Jun Yang

We are providing an unedited version of this manuscript to give early access to its findings. Before final publication, the manuscript will undergo further editing. Please note there may be errors present which affect the content, and all legal disclaimers apply.

If this paper is publishing under a Transparent Peer Review model then Peer Review reports will publish with the final article.

***METTL3-mediated m<sup>6</sup>A modification regulates CDKN1A to attenuate chronic sleep deprivation-induced cognitive impairment and neuronal apoptosis in rats***

Fei Xing<sup>1,2,#</sup>, Xiao-Shan Shi<sup>1,2,#</sup>, Han-Wen Gu<sup>1,2</sup>, Pan-Miao Liu<sup>1,2</sup>, Lei Lei<sup>1,2</sup>, Min Jia<sup>1,2</sup>, Xing-Ming Wang<sup>1,2</sup>, Mu-Huo Ji<sup>3</sup>, Jian-Jun Yang<sup>1,2,4\*</sup>

1. Department of Anesthesiology, Pain and Perioperative Medicine, The First Affiliated Hospital of Zhengzhou University, Zhengzhou, Henan, 450052, China
2. Neuroscience Research Institute, Zhengzhou University Academy of Medical Sciences, Zhengzhou, Henan, 450001, China
3. Department of Anesthesiology, The Second Affiliated Hospital of Nanjing Medical University, Nanjing, Jiangsu, 210011, China
4. Department of Anesthesiology and Perioperative Medicine, The First Affiliated Hospital of Nanjing Medical University, Nanjing 210029, China

**#These authors contributed equally.**

**\*Corresponding authors**

Jian-Jun Yang, PhD

Email: yjyangjj@126.com

Department of Anesthesiology, Pain and Perioperative Medicine, The First Affiliated Hospital of Zhengzhou University, Zhengzhou, Henan, 450052, China

## Abstract

Chronic sleep deprivation (CSD) can induce cognitive impairment, but its molecular mechanism remains unclear. In this study, initial m<sup>6</sup>A RNA sequencing of the hippocampal CA3 region in CSD rats, coupled with differential gene expression analysis of the total RNA fraction, revealed downregulation of *METTL3*, which was consistent with impaired performance in the Morris Water Maze (MWM) and confirmed by qRT-PCR and Western blot. Further investigation showed that, in HT-22 cells, *METTL3* knockdown exacerbated rapamycin-induced apoptosis. RNA sequencing of *METTL3*-knockdown cells identified gene modules and specific differentially expressed genes associated with *METTL3* loss. Differential expression analysis revealed that *CDKN1A* was significantly upregulated following *METTL3* knockdown. Methylated RNA immunoprecipitation followed by qPCR (MeRIP-qPCR) further showed that *METTL3* knockdown reduced the m<sup>6</sup>A methylation level of *CDKN1A* mRNA. *In vivo*, *METTL3* overexpression in CSD rats reduced *CDKN1A* levels, decreased neuronal apoptosis, improved spatial memory, and alleviated CA3 neuronal damage. *In vitro*, *METTL3* knockdown upregulated *CDKN1A* and promoted apoptosis in HT-22 cells, while *CDKN1A* knockdown reversed this effect. Collectively, our results demonstrate that *METTL3* downregulation promotes CSD-induced cognitive impairment by driving *CDKN1A*-dependent neuronal apoptosis, thereby identifying the *METTL3/CDKN1A* axis as a potential therapeutic target.

**Keywords:** *METTL3*, Cognitive dysfunction, Chronic sleep deprivation, m<sup>6</sup>A methylation, *CDKN1A*

## 1. Introduction

Cognitive impairment refers to the decline in cognitive functions such as memory and attention(1). Sleep deprivation exerts a detrimental impact on the hippocampus, a brain region responsible for memory and learning(2). Chronic sleep deprivation (CSD) not only impairs

cognitive functions but also increases the risk of developing cognitive disorders and mental health conditions(3). Additionally, CSD is associated with various health problems such as metabolic disorders and cardiovascular diseases, which can lead to elevated morbidity and mortality rates(4). Therefore, developing of novel diagnostic biomarkers and prognostic indicators for CSD is essential to improve cognitive impairment.

The hippocampus plays a crucial role in the formation of long-term memory, among which the CA3 subregion serves as the core for memory encoding, storage, and retrieval. A study by Ochaj J et al. demonstrated that CSD leads to impaired performance of rats in spatial memory tasks, accompanied by a reduction in the number of pyramidal cells, neuronal degeneration, and decreased Nissl substance staining intensity in the hippocampal CA3 subregion(5). Watson JF et al. investigated the cellular and microcircuit characteristics of the human hippocampal CA3 region and found that this subregion exhibits a structural feature of sparse connectivity, which optimizes memory storage capacity(6). Together, these findings suggest that the function of neurons in the hippocampal CA3 subregion may help reveal the molecular mechanisms underlying cognitive impairment.

In light of the vulnerability of the hippocampus to environmental insults, recent attention has turned to epigenetic regulation as a key mechanism underlying cognitive impairment(7). N6-methyladenosine ( $m^6A$ ) is the most abundant internal modification in eukaryotic mRNA and has become a key epitranscriptome marker in the central nervous system, which participates in neural development, synaptic plasticity, and learning-memory processes by regulating RNA metabolism(8-10). A study by Yan L et al. indicated that exercise promotes the restoration of  $m^6A$  methylation in the brain through liver metabolism, improves neural network activity, and alleviates anxiety(11). Among  $m^6A$  regulatory components, Methyltransferase 3 (*METTL3*), as a major methyltransferase, is a crucial enzyme responsible for the methylation of RNA, particularly  $m^6A$ , which is essential in modulating RNA stability, splicing, and translation(12, 13). Additionally,

*METTL3* is engaged in several brain processes, such as neurogenesis and synaptic plasticity(14), and may regulate neuronal function participating in the pathophysiological processes of cognitive impairment(15). Silencing of *METTL3* reduces the proliferation of neural stem cells and impairs neuronal maturation(14, 16). Chen H et al. have demonstrated that in an Alzheimer disease mouse model, *METTL3* alleviated cognitive impairment and mitochondrial dysfunction by upregulating mitofusin 2 (*MFN2*) expression through m<sup>6</sup>A modification(17). Together, these studies have indicated that *METTL3* is a vital part of modulating both neuronal dysfunction and neuroinflammation to protect against cognitive impairment in various disease models.

CSD is known to induce cognitive impairment, yet the underlying molecular mechanisms remain poorly understood. Increasing evidence suggests that epitranscriptomic regulation, particularly m<sup>6</sup>A modification, plays a critical role in neuronal function, stress responses, and memory formation. The methyltransferase *METTL3* plays an important role in regulating cell apoptosis, cell cycle, and RNA stability(18). Deficiency of *METTL3* prolongs the expression of pro-apoptotic genes, leading to abnormal apoptosis of cerebellar granule cells(19). Under oxidative stress, *METTL3* participates in the regulation of cellular antioxidant response and apoptosis by modulating m<sup>6</sup>A methylation(20). NSUN2 and *METTL3* can upregulate *p21* expression through m<sup>6</sup>A/m<sup>5</sup>C methylation, thereby inhibiting hydrogen peroxide-induced cell apoptosis(21). It is known that *METTL3* downregulation is associated with cognitive impairment, but the causal relationship between CSD and *METTL3* dysregulation—as well as the downstream mechanisms linking *METTL3*-dependent m<sup>6</sup>A modification to neuronal apoptosis—remains largely unclear. To address this knowledge gap, this study aims to elucidate how *METTL3* contributes to CSD-induced cognitive deficits, with a particular focus on m<sup>6</sup>A-dependent regulatory pathways and neuronal apoptosis. Through in vivo and in vitro models, potential therapeutic targets for alleviating CSD-induced cognitive decline will be explored.

## 2. Material and methods

### 2.1 CSD rats model

All animal experiments were conducted in accordance with the ARRIVE guidelines (Animal Research: Reporting of In Vivo Experiments) and the National Institutes of Health Guide for the Care and Use of Laboratory Animals. All procedures were approved by the Ethics Committee of the First Affiliated Hospital of Zhengzhou University (approval number: 2025-KY-0434-001). In this study, a total of fifty 5-week-old male SD rats were used, purchased from Wuhan Servicebio Technology Co., Ltd. (Wuhan, China). The animal study consisted of two experimental phases. Phase I included two groups (Control and CSD, n = 10 per group). Phase II included three groups (Control, CSD + vector, and CSD + over-METTL3, n = 10 per group) to evaluate the impact of *METTL3* overexpression. The randomization was implemented using a computer-generated random number table: each rat was assigned a unique number, and numbers were randomly sorted into 5 groups with equal size, ensuring no subjective selection bias. The rats were kept in soundproof rooms under controlled conditions (temperature: 24 ± 1°C, 12-hour light/dark cycle, relative humidity: 50-60%, starting at 8:00 AM) and permitted free access to standard laboratory water and food. Before the induction of CSD, all animals underwent a 3-week adaptation period. To induce CSD, a gentle method involving a rotating rod placed above the floor of the cage was used. The rats were gently nudged awake by the slow rotation of the rod, which encouraged low-level activity until the animals were fully awake. This procedure effectively induces CSD and has been validated in previous studies using behavioral wakefulness monitoring(22, 23). This procedure effectively induces CSD, as described by previous studies. The rotation was programmed to accelerate from 4 to 40 rpm over 5 minutes. Each cycle of rotation lasted 5 minutes and was applied every 30 minutes throughout the 10-hour deprivation period (from 8:00 AM to 6:00 PM). The direction of rotation was alternated periodically to minimize habituation, and rat activity was monitored to ensure wakefulness during the entire deprivation period. The CSD group was subjected to 10 hours of sleep deprivation daily (from 8:00 AM to 6:00 PM) for a total duration of 6 weeks. The sample size of 10 rats per group was determined based on previous studies investigating hippocampal cognitive function and neuronal apoptosis in rodent sleep deprivation models. Power analysis (using G\*Power 3.1 software) confirmed that this sample size achieves a

statistical power of >80% ( $\alpha=0.05$ ) to detect significant differences in key outcomes between groups, ensuring the reliability of statistical results.

## 2.2 Viral vector preparation and stereotaxic injection

For groups receiving viral injections (CSD + vector and CSD + over-*METTL3*), stereotaxic injection of adenovirus into the bilateral hippocampal CA3 region was performed immediately after the 1-week adaptation period. Following viral injection, rats were allowed a 2-week recovery period to ensure stable expression of the transgenes, after which CSD was induced. Adenovirus vectors for *METTL3* overexpression (pEZ-AV12-*METTL3*/mCherry) and the corresponding negative control vectors (pEZ-AV12-vector/mCherry) were purchased from GenePharma (GenePharma, Shanghai, China). Stereotaxic microinjection was performed as previously described(24). Briefly, rats were anesthetized with 4–5% isoflurane and maintained with 1–2% isoflurane (RWD LifeScience Co., Shenzhen, China) to ensure the stereotaxic injection procedure was performed painlessly, in line with the principle of minimizing animal suffering during experimental operations and securely placed in a stereotaxic frame. A total volume of 1.0  $\mu$ l of adenovirus suspension (0.5  $\mu$ l per side,  $2 \times 10^9$  titer units/ml diluted 10  $\times$  with enhanced infection solution) was bilaterally injected into the hippocampus using the following coordinates relative to bregma: anteroposterior (AP) -3.80 mm, mediolateral (ML)  $\pm 4.2$  mm, and dorsoventral (DV) -3.80 mm from the skull surface. The injection was performed over 5 minutes to allow for slow diffusion of the viral solution, and the needle was left in place for an additional 5-minute post-injection to minimize backflow. Rats injected with empty adenovirus vectors served as the negative control group (vector). Following the procedure, rats were allowed to recover on a heating pad until fully awake and were monitored daily for body weight, neurological status, and any signs of distress or infection. To protect the injection site, rats were housed individually for 24 hours post-surgery.

Inclusion criteria: healthy male SD rats without surgical complications and with normal pre-operative behavior. Exclusion criteria: before data analysis, animals exhibiting severe illness or signs of infection, those in which stereotaxic surgery was unsuccessful or could not be recovered,

or those with technical issues (e.g., misplacement of the injection needle) were excluded, and these predefined exclusion criteria (e.g., >20% body weight loss, postoperative neurological deficits) were recorded to ensure experimental transparency and reproducibility.

### **2.3 Morris water maze (MWM) test**

As previously mentioned, the MWM test was conducted(25). The maze consisted of a circular pool with a depth of 40 cm and a diameter of 120 cm, which was divided into four equal quadrants. The temperature of the water was maintained at  $22 \pm 1^{\circ}\text{C}$ , and the water was made opaque with the addition of milk to obscure a concealed platform in the middle of one of the quadrants, 1 cm below the water's surface. Rats underwent daily trials for 5 consecutive days for training. During each trial, animals had little more than sixty seconds to find the secret platform, and once found, they had fifteen seconds to remain on the platform. A rat was manually directed to the platform and left there for 15 seconds if it was unable to find it within the allotted 60 seconds. On Day 6, the hidden platform was removed, and an exploration test was conducted. The rats were given 60 seconds to explore the pool, and their activity was tracked using a video tracking system (Jiliang Software Technology, Shanghai, China). Spatial memory performance was quantified using: (1) Target-quadrant time: cumulative time spent in the quadrant where the platform was previously located. (2) Platform crossings: number of times the rat crossed directly over the previous platform location. These measures were used to evaluate learning and memory performance, and all data were analyzed across individual animals.

### **2.4 Hematoxylin-eosin (H&E) staining**

After the designated experimental period, rats were deeply anesthetized with an overdose of sodium pentobarbital (100 mg/kg, intraperitoneally) and transcardially perfused with 0.9% saline, followed by 4% paraformaldehyde (PFA, P1110, Solarbio, China) in phosphate-buffered saline (PBS, pH 7.4). Craniotomy was performed to extract whole brains, which were post-fixed in the same fixative at  $4^{\circ}\text{C}$  for 24 hours. Using stereotaxic coordinates from Paxinos and Watson rat brain

atlas (2007), the hippocampal CA3 subregion was identified and microdissected. The brain tissues containing the hippocampal CA3 region of the rats were sectioned, paraffin-embedded, and fixed in 4% paraformaldehyde for 24 hours. The stained hippocampal CA3 region sections were hydrated in a series of ethanol solutions (100%, 95%, 85%, and 70%) for 5 minutes each. Following this, the sections were given three five-minute washes in tap water. After 10 minutes of hematoxylin staining, the slices were rinsed with water, differentiated with 1% hydrochloric acid alcohol for 10 seconds, rinsed with water again, and then rinsed with running water after 0.6% ammonia became blue. After three minutes in the eosin dying solution, the slices were dehydrated with ethanol and xylene to make them transparent, then air-dried for neutral gum sealing. Finally, the stained hippocampal CA3 region sections were examined by an Olympus light microscope in Tokyo, Japan.

## 2.5 Nissl staining

The brain tissues containing the hippocampal CA3 region of the rats were hydrated in a series of ethanol solutions. Following this, three rounds of five-minute washings were performed on each section. The tissue was then stained with 0.1% cresyl violet (41830-80-2, Sigma-Aldrich, Germany) for 10 minutes. Following staining, distilled water was used to rinse the sections, followed by a gradient of alcohol solutions to dehydrate them and xylene to clarify them. Finally, the sections were mounted using neutral gum. The stained sections were imaged using an Olympus VS120 Virtual Slide Scanner. The damaged neurons in the CA3 area were seen to be sickle-shaped, undersized, and highly stained, sometimes with fragmented or nonexistent nuclei, in contrast to normal neurons that were uniformly shaped and stained. The percentage of injured neurons in the CA3 area was calculated to assess the impact of sleep deprivation on hippocampal neuronal structure. For quantification, the region of interest (ROI) was defined as the cell-dense neuronal layer of the hippocampal CA3 region in each section. Neuronal counting was performed using automated segmentation in ImageJ software (version 2.0.0). To reduce subjectivity, brightness and contrast thresholds were first set on pilot images and then fixed across all images within the same

staining batch. Automated counts were validated against manual counts for a subset of images ( $n = 15$ ), yielding high concordance (Pearson  $r > 0.9$ ). Counting was performed by an investigator blinded to the experimental groups. Only neurons with clearly visible nuclei were included, while ambiguous or overlapping cells were excluded. The percentage of injured neurons within the defined ROI was calculated to assess the impact of sleep deprivation on hippocampal neuronal structure.

## 2.6 Cell line and culture conditions

The Chinese Academy of Sciences Cell Bank (Shanghai, China) provided the mouse hippocampus neuronal cell line HT-22 cells. A complete medium consisting of 90% Dulbecco's Modified Eagle's Medium (11995065, DMEM, Gibco, USA) and 10% fetal bovine serum (A5669701, FBS, Thermo Fisher scientific, USA) was employed to cultivate HT-22 cells. The cells were cultured in a humidified incubator at 37°C with an atmosphere of 5% CO<sub>2</sub>.

## 2.7 Cell transfection and treatment

HT-22 cells were planted at a density of  $2 \times 10^5$  cells per well in 24-well plates and cultured overnight in complete growth medium to achieve approximately 70-80% confluency. Following the manufacturer's guidelines, Lipofectamine 2000 transfection reagent (11668019, Invitrogen, Shanghai, China) was utilized. Specifically, small interfering RNAs (siRNAs) targeting *METTL3* (si-*METTL3*-1 and si-*METTL3*-2), targeting *CDKN1A* (si-*CDKN1A*), or a negative control siRNA (si-NC), as well as plasmids encoding *CDKN1A* for overexpression, were all purchased from GenePharma (Shanghai, China) and transfected into HT-22 cells. The control group was transfected with an empty vector (vector, GenePharma, Shanghai, China) under the same conditions. All transfection procedures followed a standardized protocol as per the manufacturer's guidelines. Cells were harvested for subsequent experimentation after 48 hours of transfection. Rapamycin (Rap, S1039, Selleck, Houston, USA) was dissolved in dimethyl sulfoxide (DMSO) to generate a 10 mM stock solution. Before experimental treatment, the stock solution was further

diluted in a full culture medium to 50 µg/ml as the ultimate concentration. Rap was administered to HT-22 cells for four hours at a dosage of 50 µg/ml(26).

## **2.8 m<sup>6</sup>A RNA sequencing analysis of rat hippocampal CA3 tissues**

Total RNA was extracted from rat hippocampal CA3 tissues, including both control and CSD groups, using TRIzol reagent (R110, Solarbio, Beijing, China) following the manufacturer's instructions. The concentration and purity of the RNA were measured using a NanoDrop 2000 spectrophotometer (Thermo Scientific, Shanghai, China), and RNA integrity was assessed with an Agilent 2100 Bioanalyzer (Agilent, Shanghai, China). For m<sup>6</sup>A RNA sequencing, methylated RNA immunoprecipitation (MeRIP) was performed using the GenSeq™ m<sup>6</sup>A-MeRIP Kit (GenSeq, China) according to the manufacturer's protocol to enrich m<sup>6</sup>A-modified RNA fragments. The enriched RNA fragments were then used to construct sequencing libraries. Library preparation and sequencing were carried out by Majorbio Bio-Pharm Technology Co., Ltd. (Shanghai, China). Sequencing was performed on the Illumina NovaSeq 6000 platform, generating high-throughput, high-quality data for downstream m<sup>6</sup>A peak identification and differential methylation analysis.

## **2.9 RNA sequencing analysis of HT-22 cells transfected with si-*METTL3-1* plasmids**

Total RNA was extracted from HT-22 cells transfected with si-*METTL3-1* and si-NC (negative control) plasmids using TRIzol reagent, following the manufacturer's instructions. RNA concentration, purity, and integrity were measured using NanoDrop 2000 and Agilent 2100 Bioanalyzer, respectively. RNA sequencing libraries were prepared using the VAHTS Universal V6 RNA-seq Library Prep Kit (Vazyme, China) according to the manufacturer's protocol. Library construction and sequencing were performed by Majorbio Bio-Pharm Technology Co., Ltd. on the Illumina NovaSeq 6000 platform, providing high-quality transcriptome data for analyzing the effects of *METTL3* knockdown.

## **2.10 Dataset source and differential expression analysis**

This study generated two sequencing datasets: m<sup>6</sup>A RNA-seq and RNA-seq. The m<sup>6</sup>A RNA-seq dataset included three control (normal rat) samples and three CSD (CSD rat) samples. The RNA-seq dataset consisted of three samples treated with si-NC (control group) and three samples transfected with si-METTL3-1 (si-METTL3 group). Differential expression analysis of genes was conducted separately for both datasets using the "limma" package in R software (version 4.1.0, <https://www.r-project.org/>). Genes were selected based on fold change (FC), with upregulated differentially expressed genes (DEGs) defined as those with FC > 2, and downregulated DEGs defined as those with FC < 0.5. Statistical significance was determined using the P < 0.05 criterion.

## 2.11 Hierarchical clustering analysis

Hierarchical clustering analysis was performed to assess the similarity among the 92 DEGs in the m<sup>6</sup>A RNA-seq dataset. The clustering results were visualized as a dendrogram, representing the pairwise relationships between arrays. The similarity between two arrays was measured by their correlation coefficient, with the association inversely related to the distance between the arrays. The clustering algorithm identified pairs of arrays with the smallest distance and linked them into clusters, with the distance between arrays defined as one minus their correlation. The algorithm iteratively built the tree structure by progressively merging the closest clusters, resulting in a binary hierarchical tree.

## 2.12 Weighted gene co-expression network analysis (WGCNA)

Weighted Gene Co-expression Network Analysis (WGCNA) was performed on the RNA-seq data to identify co-expressed gene modules. The co-expression network for all genes was constructed using the Bioinfo Intelligent Cloud platform (<https://www.bic.ac.cn/BIC/#/>). A scale-free network was built using a soft threshold with  $\beta = 18$ . Genes were clustered into several modules based on their co-expression patterns, with different colors representing each module. The two most strongly correlated modules were selected for further analysis. We detected module membership (MM) and gene significance (GS) to assess the stability of the identified modules.

### **2.13 Gene overlapping identification**

To identify overlapping genes between DEGs from the RNA-seq data and the two most strongly correlated modules identified through WGCNA, we conducted a topological analysis using the Venn Online Graph Tool (<https://bioinformatics.psb.ugent.be/webtools/Venn/>).

### **2.14 Functional enrichment analysis**

Functional enrichment analysis was conducted using Enrichr (<https://maayanlab.cloud/Enrichr/>) to investigate the biological relevance of DEGs identified from m<sup>6</sup>A RNA-seq data of CSD rat models and controls. This comprehensive analysis included Kyoto Encyclopedia of Genes and Genomes (KEGG) pathway and biological process (BP) enrichment. The GO classification system classifies gene and protein functions into three major hierarchical categories: BP, molecular function (MF), and cellular component (CC). In addition, GO (BP, CC, MF) and KEGG pathway enrichment analyses were conducted on DEGs identified from RNA sequencing data of HT-22 cells transfected with si-NC and si-METTL3-1.

### **2.15 Expression analysis and visualization**

Expression levels of *METTL3* in the m<sup>6</sup>A RNA-seq dataset, as well as the expression of overlapping genes in the RNA-seq data from HT-22 cells transfected with si-NC and si-METTL3-1, were analyzed using the Sangerbox platform (version 3.0, <http://vip.sangerbox.com/home.html>). First, the expression of *METTL3* was assessed in both the control and CSD groups from the m<sup>6</sup>A RNA sequencing data. Subsequently, the expression of overlapping genes was analyzed between the si-NC and si-METTL3-1 groups within the RNA-seq dataset. When  $P < 0.05$ , the results obtained are significant.

### **2.16 Quantitative real-time PCR (qRT-PCR) analysis**

Following the manufacturer's instructions, total RNA was extracted from rat hippocampal

tissue and mouse neurons with TRIzol reagent (R110, Solarbio, Beijing, China). The concentration and purity of RNA were assessed employing a NanoDrop 2000 spectrophotometer (Thermo Scientific, Shanghai, China). Following the manufacturer's instructions, the process transformed 1 µg of total RNA into complementary DNA (cDNA) with the PrimeScript RT Master Mix Kit (RR036A, Takara, Japan). By a StepOnePlus Real-Time PCR System (Applied Biosystems, USA) and SYBR Green PCR Master Mix (639676, Takara, Dalian, China), qRT-PCR was carried out. The relative gene expression was calculated using the  $2^{-\Delta\Delta CT}$  method(27). For rat hippocampal tissue samples, the following primers were used: *METTL3* forward: 5'-ATCCCCAAGGCTTCAACAG-3', *METTL3* reverse: 5'-ATCCAGTTGGGCTGCACATT-3' and *GAPDH* forward: 5'-ACGGGAAACCCATCACCATC-3', *GAPDH* reverse: 5'-TCACAAACATGGGGGCATCA-3'. For HT-22 cells, the following primers were used: *METTL3* forward: 5'-GTCTGCCATCTCTACGCCA-3', *METTL3* reverse: 5'-TCATGGCAGACAGCTTGGAG-3', *CDKN1A* forward: 5'-TAAGGACGTCCCACTTGCC-3', *CDKN1A* reverse: 5'-AAAGTTCCACCGTTCTCGGG-3', and *GAPDH* forward: 5'-GGGTCCCAGCTTAGGTTCAT-3', *GAPDH* reverse: 5'-TGAGGTCAATGAAGGGTCA-3'. The *GAPDH* gene was used as the internal reference for both rat and mouse samples.

*GAPDH* was used as the internal reference for normalization. Primer efficiency (90–110%) and linearity were confirmed using standard curves, and melting curve analysis verified product specificity. Each reaction was run in triplicate, and statistical analyses were based on biological replicates. Only data within the linear amplification range were used for quantification.

## 2.17 Western blot (WB) analysis

Protein lysates were prepared from rat hippocampal tissue and mouse neurons utilizing RIPA lysis buffer (#P0013B, Beyotime, China) with protease and phosphatase inhibitors added. The BCA Protein Assay Kit (Bioteke, Beijing, China) was applied to detect the protein concentration. After being separated by SDS-PAGE, equal quantities of protein were transferred to PVDF membranes (#P0965-20pcs, Beyotime, China). The membranes were then incubated with primary

antibodies: anti-METTL3 (1:1000, ab195352, Abcam, Cambridge, UK), anti-CDKN1A (1:1000, ab109199, Abcam, Cambridge, UK), anti-Bax (1:1000, ab32503, Abcam, Cambridge, UK), anti-Caspase3 (1:2000, ab184787, Abcam, Cambridge, UK), anti-Cleaved Caspase3 (1:2000, ab184787, Abcam, Cambridge, UK) and anti-GAPDH (1:10000, ab181602, Abcam, Cambridge, UK), all of which were purchased from Abcam, Cambridge, UK. After incubation with primary antibodies, the membranes were incubated with Goat Anti-Rabbit IgG H&L (HRP, 1:2000, ab6721, Abcam, Cambridge, UK) secondary antibody. A technique for ECL detection (#P0018S, Beyotime, Shanghai, China) was utilized to observe protein bands. Images were captured and analyzed using ImageJ software (version 2.0.0).

GAPDH was used as the loading control to ensure equal protein loading and normalization across samples. Exposure times were optimized to maintain signals within the non-saturating range, and each blot was confirmed to show linear signal intensity with increasing protein load. Band intensities were quantified using ImageJ after background subtraction. All analyses were based on at least three independent biological replicates, with technical duplicates for each sample to ensure reproducibility.

## 2.18 Flow cytometry analysis

Flow cytometry was used to detect apoptosis in HT-22 cells. Initially, HT-22 cells were planted at a density of  $1 \times 10^4$  cells per well in 24-well plates. After dissociation with 0.25% trypsin-EDTA (25200056, Thermo Fisher Scientific, Inc.) and washing with PBS (C0221A, Beyotime, China), cells were incubated with 5  $\mu$ l of PI solution and 5  $\mu$ l of Annexin V-FITC for 15 minutes at room temperature to assess apoptosis. Following staining, a flow cytometer (ACEA NovoCyte 2060R, China) was used to detect the fluorescence of Annexin V-FITC and PI, and FlowJo software (version 10.6.0, FlowJo software, Oregon, USA) was applied for data analysis.

## 2.19 m<sup>6</sup>A-RNA Immunoprecipitation followed by qRT-PCR (MeRIP-qPCR)

To assess the impact of *METTL3* knockdown on m<sup>6</sup>A modification of *CDKN1A* mRNA, m<sup>6</sup>A-

RIP followed by qRT-PCR was performed. Total RNA was extracted using TRIzol reagent and treated with DNase I to remove genomic DNA contamination. RNA was fragmented according to the mRNA Fragmentation Protocol provided by New England Biolabs (NEB, Beijing, China), typically by incubating at 94°C for 5 minutes in fragmentation buffer. Fragmented RNAs were subjected to immunoprecipitation with m<sup>6</sup>A-specific antibody (Active Motif, Beijing, China) or IgG antibody (1:1000, ab172730, Abcam, Cambridge, UK) using the EpiMark N6-Methyladenosine Enrichment Kit (E1610S, New England Biolabs, USA), following the manufacturer's instructions. After immunoprecipitation, RNA was purified and reverse-transcribed, followed by qPCR amplification. *GAPDH* mRNA was analyzed in parallel as a non-enriched internal control. m<sup>6</sup>A enrichment was calculated, normalized to input RNA and IgG control.

## 2.20 RNA stability assay

To evaluate the stability of *CDKN1A* mRNA, actinomycin D (SBR00013, Sigma-Aldrich, Germany) was used following *METTL3* knockdown in HT-22 cells. As previously indicated, the test was performed. Actinomycin D was administered at a final 2 µg/mL concentration when the cells achieved 80% confluence. Following treatment, cells were then taken at 0, 2, 4, 6, and 8 hours. Total RNA was extracted from the cells, and RNA stability was assessed by qRT-PCR.

## 2.21 Statistical analysis

The GraphPad Prism software (version 8.1.0) was applied to assess the data. Each experiment was conducted three times, and all data are presented as the mean ± standard error of the mean (SEM). Data were tested for normality using the Shapiro–Wilk test and for homogeneity of variance using Levene's test. The differences between two groups were examined with the Student's *t*-test. For multiple group comparisons, after testing for homogeneity of variance using Levene's test as mentioned above, one-way analysis of variance (ANOVA) with Tukey's or Bonferroni's post hoc test was utilized for multiple group comparisons. For data involving

repeated measurements over time within the same samples, repeated measures ANOVA was performed to assess statistical differences. The assumption of sphericity was evaluated using Mauchly's test, and when violated ( $p < 0.05$ ), the Greenhouse–Geisser correction was applied to adjust the degrees of freedom.  $P < 0.05$  was regarded as statistically significant.

### 3. Results

#### 3.1 METTL3 is significantly down-regulated in the hippocampal CA3 region of CSD rats

To investigate m<sup>6</sup>A methylation and concurrent gene expression changes in CSD rats, we performed m<sup>6</sup>A RNA-seq on rat hippocampal CA3 tissues. We evaluated m<sup>6</sup>A RNA-seq data quality via genome region distribution and gene body coverage analyses. The reads distribution histogram (Supplementary Figure 1A) showed all samples (control: 1-3, CSD: 1-3) had  $> 60\%$  of reads enriched in CDS, with low proportions in other regions (e.g., TSS flanking regions, UTR, intergenic regions, introns), indicating high transcript capture specificity. The gene body coverage curve (Supplementary Figure 1B) confirmed consistent patterns across samples: coverage peaked in the middle gene body ( $\approx 20\text{--}60$  th percentile, 5'→3') and gradually declined toward the 3' end, consistent with typical RNA-seq characteristics, verifying data reliability and reproducibility. The m<sup>6</sup>A RNA-seq analysis of rat hippocampal CA3 tissues revealed 43 significantly downregulated and 49 upregulated DEGs between control and CSD groups (**Figure 1A**), with *METTL3* exhibiting marked downregulation (indicated in red). Hierarchical clustering analysis of gene expression profiles further confirmed the obvious differences between the CSD group (n=3) and the control group (n=3) (**Figure 1B**). GO analysis was then conducted to identify enriched biological processes (BP), and the enriched items included "Negative regulation of cell cycle (GO: 0045786)", "Regulation of hormone secretion (GO: 0046883)", "Mitotic G2/M transition checkpoint (GO: 0044818)", etc (**Figure 1C**). These processes indicated that CSD exposure may influence cell cycle progression and differentiation. KEGG pathway analysis revealed 5 significantly enriched pathways, including "Phenylalanine, tyrosine and tryptophan biosynthesis", "Phenylalanine metabolism", "Oxytocin signaling pathway", and "Melanoma" (**Figure 1D**). Finally, the

expression level of *METTL3* was analyzed, and the findings indicated that *METTL3* expression in the CSD group markedly declined in comparison to the control group, suggesting that it might be involved in the CSD response (**Figure 1E**).

### **3.2 *METTL3* is downregulated in the hippocampal CA3 region in the CSD-induced cognitive impairment**

Following the 6-week CSD modeling period, MWM tests were conducted immediately to assess cognitive function. A schematic timeline of the experimental procedure is presented in **Figure 2A**. The trajectory patterns for both the control and CSD groups are shown in **Figure 2B**. While the control group exhibited a typical path toward the target platform, the CSD group showed a more erratic trajectory. The frequency of crossing the platform (**Figure 2C**) was substantially lower in the CSD group than in the control group, indicating impaired cognitive performance in CSD-exposed animals. In addition, the CSD group spent a notably less amount of time in the target quadrant (**Figure 2D**) during the MWM test, further confirming the cognitive deficits induced by CSD exposure. Notably, differential gene expression analysis based on total RNA signals from m<sup>6</sup>A RNA-seq identified *METTL3* as exhibiting significant downregulation in the hippocampal CA3 region of CSD rats. Moreover, *METTL3* has been extensively studied in the context of hippocampal function and related neurological processes. To investigate the molecular changes underlying these cognitive impairments, we measured the relative mRNA expression of *METTL3*. As shown in **Figure 2E**, *METTL3* mRNA expression was significantly lower in the CSD group compared to the control group, indicating that *METTL3* might contribute to CSD-induced cognitive dysfunction. WB analysis also showed a similar pattern, with the CSD group's *METTL3* protein expression significantly lower than that of the control group (**Figures 2F and 2G**). These findings highlight a potential link between *METTL3* downregulation and impaired cognitive function following CSD exposure.

### **3.3 *METTL3* knockdown increases Rap-induced apoptosis in HT-22 cells**

To explore the function of *METTL3* in neurons, *METTL3*-specific siRNAs were transfected in HT-22 cells, and the effective knockdown of *METTL3* was confirmed by qRT-PCR and WB experiments (**Figures 3A-3C**). Among the si-*METTL3* plasmids, si-*METTL3*-1 exhibited higher knockdown efficiency, and therefore, si-*METTL3*-1 was chosen for further research. To determine the optimal concentration of rapamycin for subsequent experiments, CCK8 assay was performed to detect the cell viability of HT-22 cells treated with different concentrations of rapamycin. The results showed that cell viability decreased in a concentration-dependent manner with the increase of rapamycin concentration. When the concentration of rapamycin reached 50 µg/mL, the cell viability was approximately 50%, which was selected as the effective intervention concentration for subsequent experiments (**Figure 3D**). To evaluate the impact of *METTL3* knockdown on apoptosis, HT-22 cells were treated with Rap by flow cytometry analysis. The outcomes demonstrated that the apoptosis rate increased after Rap treatment alone, and the apoptosis rate was further enhanced after the knockdown of *METTL3* on this basis, suggesting that *METTL3* knockdown could enhance Rap-induced apoptosis (**Figures 3E and 3F**). In addition, WB analysis identified Caspase-3, cleaved Caspase-3 and Bax expression, three proteins linked to apoptosis (**Figures 3G-3I**). The outcomes proved that Bax and cleaved Caspase-3 in the Rap+si-*METTL3*-1 group were considerably raised, confirming the function of *METTL3* in regulating apoptosis.

### 3.4 WGCNA identifies key gene co-expression modules associated with *METTL3* knockdown in HT-22 cells

We performed WGCNA on RNA-seq data of *METTL3* knockdown in HT-22 cells. Sample clustering showed that samples were clustered into different groups according to treatment, and no significant outliers were detected (**Figure 4A**). 18 was found to be the network's optimal soft threshold, and the scale-free topological fit index was 0.85 (**Figure 4B**). The dynamic tree cutting and resulting module colors were allocated to different gene co-expression modules (**Figure 4C**). These modules were then analyzed for their relationship with *METTL3* knockdown (**Figure 4D**). The eigenvalue adjacency heatmap demonstrated the correlation between modules and revealed

strong adjacency within the modules, especially the MEbrown and MEGreen modules (**Figure 4E**). Of these, the correlation coefficient between module members and gene importance (si-NC) of MEbrown was 0.99 (**Figure 4F**). The correlation coefficient between module members and gene importance (si-METTL3-1) of MEGreen module was 0.93 (**Figure 4G**). These module-specific correlations suggest that the MEbrown and MEGreen modules may represent gene clusters functionally involved in *METTL3*-associated molecular responses. Further enrichment analysis of these modules may help to identify pathways related to m<sup>6</sup>A-mediated neuronal regulation or stress responses.

### 3.5 Differential gene expression and pathway analysis in *METTL3* knockdown cells

Differential gene expression analysis was conducted after knockdown of *METTL3* in HT-22 cells. 171 upregulated DEGs and 50 downregulated DEGs were obtained, of which 14,634 genes did not change significantly (**Figure 5A**). A total of nine overlapping genes between the DEGs and WGCNA modules were identified, with seven derived from the green module and two from the brown module. (**Figure 5B**). GO analysis revealed that the pathways enriched in these overlapping genes included "DNA damage response (GO:0006974)", "Mitotic G1 DNA damage checkpoint signaling (GO:0031571)", DNA damage response (GO:0006974)", "Mitotic G1 DNA damage checkpoint signaling (GO:0031571)", and "Lysophosphatidic acid acyltransferase activity (GO:0042171)", etc (**Figure 5C**). These outcomes indicated that *METTL3* knockdown may affect DNA damage response and cell cycle regulation. Additionally, KEGG pathway analysis indicated a significant enrichment in the "p53 signaling pathway" (**Figure 5D**), further supporting the role of *METTL3* in cell cycle and apoptosis-related pathways. Finally, we validated the expression levels of these nine overlapping genes, including *PRELP*, *BTG2*, *ANXA8*, *CDKN1A*, *CDSN*, *INKA2*, *PIDD1*, *CES2E*, and *CRLS1*. As shown in **Figure 5E**, *PRELP*, *BTG2*, *ANXA8*, *CDKN1A*, *INKA2*, *PIDD1*, *CES2E* were upregulated after *METTL3* knockdown, while *CDSN* and *CRLS1* were downregulated. Among these, *CDKN1A* exhibited a more pronounced expression between the two groups and was therefore selected for subsequent experimental validation. These results

further confirmed the molecular effects of *METTL3* knockdown on gene expression.

### **3.6 Effect of *METTL3* knockdown on *CDKN1A* expression and m<sup>6</sup>A modification in HT-22 cells**

The impact of *METTL3* knockdown on *CDKN1A* expression was examined by WB and qRT-PCR in HT-22 cells. In contrast with the si-NC group, both the mRNA and protein levels of *CDKN1A* were upregulated in the si-*METTL3*-1 group (**Figures 6A-6C**). Further analysis was conducted to determine the impact of *METTL3* knockdown on the m<sup>6</sup>A modification of *CDKN1A* mRNA. The results revealed a substantial decrease in m<sup>6</sup>A enrichment on *CDKN1A* mRNA following *METTL3* knockdown (**Figure 6D**). Previous research has revealed that RNA m<sup>6</sup>A methylation plays a role in regulating RNA stability(28). To assess the stability of *CDKN1A* mRNA, actinomycin D was used following *METTL3* knockdown in HT-22 cells. The outcomes revealed that the si-*METTL3*-1 group's *CDKN1A* mRNA stability was higher than that of the si-NC group (**Figure 6E**). These findings imply that *METTL3* regulates *CDKN1A* expression by modulating the m<sup>6</sup>A-mediated RNA degradation process.

### **3.7 Impact of *METTL3* overexpression on *CDKN1A* expression and apoptotic pathways in the hippocampal CA3 region of CSD rats**

To investigate the effect of *METTL3* overexpression in CSD-induced cognitive impairment rats, an adenovirus vector encoding *METTL3* and the fluorescent reporter mCherry was injected into the hippocampal CA3 region. The mCherry fluorescence was examined to assess the accuracy of CA3 targeting and the efficiency of viral transduction. Robust red fluorescence signals were detected in the CA3 region, indicating successful viral delivery and effective *METTL3* overexpression in the cells (Supplementary Figure 1C). To assess the function of *METTL3* in regulating *CDKN1A* and hippocampal CA3 region tissue changes in CSD rats, WB analysis was applied to evaluate the levels of *METTL3* and *CDKN1A* proteins in the hippocampal CA3 region following *METTL3* overexpression. Investigations demonstrated that in the hippocampal CA3

region of CSD rats, CDKN1A expression increased whereas METTL3 expression decreased. However, upon *METTL3* overexpression, METTL3 expression was partially restored, and CDKN1A levels significantly decreased (**Figures 7A-7C**). Subsequently, the levels of apoptosis-related proteins in the hippocampal CA3 region of CSD rats were evaluated. The results showed an increase in Bax and cleaved Caspase-3 levels in the hippocampal CA3 region, indicating that CSD may activate pro-apoptotic pathways, leading to neuronal apoptosis in the hippocampal CA3 region (**Figures 7D-7F**). Interestingly, after *METTL3* overexpression, cleaved Caspase-3 and Bax levels were suppressed in the hippocampal CA3 region of CSD rats (**Figures 7G-7I**). These findings suggest that *METTL3* overexpression modulates apoptosis-related pathways in the hippocampal CA3 region, potentially through the regulation of *CDKN1A* expression.

### **3.8 *METTL3* overexpression mitigates cognitive dysfunction and hippocampal neuronal damage in CSD rats**

To further evaluate the impact of CSD and *METTL3* overexpression on cognitive function, the MWM test was used to evaluate the trajectory patterns of rats. The control group exhibited a typical, stable path toward the target platform, frequently crossing the platform and spending more time in the target quadrant. In contrast, the CSD + vector group showed fewer stable trajectories, with less time spent in the target quadrant and a lower number of platform crossings. Compared with CSD + vector group, the CSD + over-*METTL3* group demonstrated more stable and direct paths toward the target platform. These rats traversed the platform more frequently and spent more time in the target quadrant, indicating that *METTL3* overexpression could reverse the cognitive deficits induced by CSD (**Figures 8A-8C**). Next, the hippocampal CA3 region cells' pathogenic alterations were observed by H&E staining. The results showed that the cells in the CA3 region of the hippocampus in the CSD + vector group were more severely atrophied in contrast to the control group. Conversely, the cells atrophy in the CA3 region of the CSD + over-*METTL3* group was less pronounced, suggesting that *METTL3* overexpression partially alleviates the neuronal damage caused by CSD (Figure 8D). Nissl staining was used to assess the structural damage to

hippocampal neurons in the CA3 region. In contrast to the control group, the CSD + vector group revealed a reduction in the number of Nissl-stained neurons, with irregular distribution. In contrast, the CSD + over-*METTL3* group demonstrated an increase in the number of neurons in the CA3 region, with a more even distribution of Nissl bodies (Figures 8E and 8F). These outcomes imply that *METTL3* overexpression may restore neuronal damage induced by CSD, improving neuronal survival and function.

### **3.9 *METTL3* knockdown promotes neuronal apoptosis through the *CDKN1A* dependent pathway in HT-22 cells**

To explore the role of *CDKN1A* in hippocampal neurons, we first transfected HT-22 cells with a *CDKN1A* overexpression plasmid. Western blot and qRT-PCR analyses validated successful *CDKN1A* overexpression (Figures 9A-9C). We then examined whether *METTL3* regulates *CDKN1A* expression. As shown in Figures 9D-9F, *CDKN1A* overexpression markedly elevated *CDKN1A* levels, and this effect was further enhanced by concurrent *METTL3* knockdown, suggesting that *METTL3* may suppress *CDKN1A* expression. Flow cytometry analysis revealed that *CDKN1A* overexpression alone promoted apoptosis, and *METTL3* knockdown further exacerbated this pro-apoptotic effect (Figures 9G and 9H). A control group (si-NC + over-*CDKN1A*) confirmed that the enhanced apoptosis was specifically due to *METTL3* knockdown rather than non-specific siRNA effects.

To definitively establish whether *CDKN1A* acts as a downstream mediator of *METTL3* in neuronal apoptosis, *CDKN1A* knockdown and *METTL3/CDKN1A* co-knockdown experiments were performed. Transfection with si-*CDKN1A* effectively reduced *CDKN1A* expression at both mRNA and protein levels (Figures 9I-9K). We then assessed the consequences of co-knockdown. *METTL3* knockdown alone (si-*METTL3* + si-NC) significantly increased *CDKN1A* expression, whereas simultaneous knockdown of both *METTL3* and *CDKN1A* (si-*METTL3* + si-*CDKN1A*) reversed this upregulation, restoring *CDKN1A* to near-control levels (Figures 9L-9N). Consistent

with these molecular changes, flow cytometry analysis demonstrated that the dramatic pro-apoptotic effect of *METTL3* knockdown was reversed by concurrent *CDKN1A* knockdown (**Figures 9O-9P**). Together, these data indicate that *METTL3* knockdown promotes neuronal apoptosis primarily by upregulating *CDKN1A*, and that *CDKN1A* is an essential downstream effector in this regulatory pathway.

#### 4. Discussion

This study aimed to elucidate the mechanistic role of *METTL3*-mediated m<sup>6</sup>A RNA methylation in cognitive impairment induced by CSD. We demonstrated that CSD causes significant spatial learning and memory deficits in rats, accompanied by a marked downregulation of *METTL3* expression in the hippocampal CA3 region. Mechanistically, *METTL3* modulates m<sup>6</sup>A modification of *CDKN1A* mRNA in hippocampal neurons, thereby regulating its expression. Reduced *METTL3* activity during CSD leads to increased *CDKN1A* levels, which in turn activate downstream pro-apoptotic factors Bax and cleaved caspase-3, ultimately triggering neuronal apoptosis. This cascade contributes to neuronal damage and the observed cognitive deficits (**Figure 10**). Critically, *METTL3* overexpression reversed these effects, restoring *CDKN1A* homeostasis, suppressing apoptosis, and rescuing cognitive deficits. This *METTL3-CDKN1A* axis highlights how sleep deprivation disrupts m<sup>6</sup>A-dependent RNA stability to amplify apoptotic signaling. Together, these results indicate that *METTL3* exerts a neuroprotective effect in CSD-induced cognitive dysfunction, likely by modulating *CDKN1A*-mediated apoptotic pathways via m<sup>6</sup>A-dependent mechanisms.

Cognitive dysfunction, characterized by impairments in memory, perception, and thinking, arises from abnormalities in the cerebral cortex's function and structure(29). Numerous studies have highlighted a strong association between sleep deprivation and cognitive decline. For instance, Csipo T et al. have demonstrated that 24-hour sleep deprivation significantly impaired cognitive performance, altered blood flow responses in the prefrontal and somatosensory cortices, and

caused the right middle cerebral artery's cerebral blood flow to decrease(30). Additionally, research by Tang H et al. has indicated that the natural compound Osthole, through activation of the Nrf2/HO-1 pathway, notably improved cognitive performance in CSD rats, restored antioxidant enzyme activity, and reversed neuronal damage in the hippocampal CA1 region(31). Similarly, Wang X et al. have found that melatonin alleviated cognitive deficits and hippocampal inflammation induced by sleep deprivation by modulating gut microbiota and metabolic products(32). Our investigation created a CSD rat model and performed gene sequencing of hippocampal cells to explore underlying molecular mechanisms. Differential expression, hierarchical clustering, and enrichment analysis of the sequencing data identified *METTL3* as a hub gene significantly downregulated in CSD rats. Behavioral testing using the MWM revealed pronounced cognitive deficits in CSD rats, accompanied by a reduction in *METTL3* expression in their hippocampi. The observations imply that *METTL3* could be essential in sleep deprivation-induced cognitive dysfunction and hippocampal alterations.

*METTL3* plays a critical role in post-transcriptional RNA modifications, influencing gene expression within cells(33). Several studies have suggested that dysregulated expression or dysfunction of *METTL3* may contribute to cognitive impairments, particularly those associated with neurodevelopmental, neuroinflammatory, and neurodegenerative disorders(34, 35). *METTL3* forms a complex with *METTL14*, which catalyzes the addition of N6-methyladenosine ( $m^6A$ ) modifications to RNA molecules, thereby mediating the majority of  $m^6A$  methylation on mRNA transcripts. For example, Huang H et al. have reported aberrant  $m^6A$  methyltransferase *METTL3* and *RBM15B* expression in the hippocampus of Alzheimer's disease (AD) patients(36). *METTL3* accumulation in the insoluble fraction was found to correlate with insoluble Tau protein levels, suggesting that abnormal *METTL3* expression and distribution could contribute to AD pathology through epitranscriptomic mechanisms. Similarly, He B et al. have demonstrated that the anesthetic isoflurane reduced *METTL3* phosphorylation in the hippocampus by inhibiting the MAPK/ERK pathway, disrupting  $m^6A$  RNA methylation signals, and potentially affecting postoperative

cognitive dysfunction (POCD)(37). Moreover, Ming Y et al. have identified that *METTL3* stabilizes *MALAT1* expression by promoting m<sup>6</sup>A modification in a mouse model of autism, which activates the Wnt/β-catenin signaling pathway and alleviates autism-like behaviors while inhibiting hippocampal neuronal apoptosis(38). In our study, rapamycin was used to induce neuronal injury. We selected rapamycin based on accumulating evidence that CSD disrupts mTOR signaling, and aberrant mTOR activation contributes to neuronal apoptosis, oxidative stress, and synaptic dysfunction in sleep-deprived brains(39, 40). As a well-characterized mTOR inhibitor, rapamycin provides a controllable and reproducible in vitro model to mimic downstream effects of mTOR dysregulation under CSD conditions. Moreover, previous studies have shown that rapamycin induces autophagy-associated apoptosis and oxidative stress in neuronal cells, partially recapitulating the cellular injury mechanisms relevant to CSD(41, 42). Our study reveals that Rap-induced inhibition of the mTOR pathway and *METTL3* knockdown enhance cleaved caspase-3 and Bax levels, thereby promoting apoptosis. Moreover, *METTL3* knockdown further exacerbates these effects, suggesting that *METTL3* may regulate neuronal survival and apoptosis in the hippocampus, potentially contributing to the pathology of cognitive deficits associated with CSD.

To further investigate the underlying mechanisms of *METTL3* in hippocampal neurons, we performed sequencing analysis on HT-22 cells treated with *METTL3* knockdown. Using WGCNA, correlation analysis, and differential expression analysis, we identified nine candidate genes linked to *METTL3* from key module genes and DEGs. Enrichment and expression analyses of these candidate genes led us to select *CDKN1A*, a downstream gene with higher expression levels, for further investigation. Previous studies have shown that *METTL3* deficiency promotes the migration, proliferation, and drug resistance of breast cancer cells by modulating the *CDKN1A/AKT* pathway, epithelial-mesenchymal transition (EMT), and the m<sup>6</sup>A-BAX/caspase-9/-3/-8 signaling pathways(43, 44). Moreover, Yao FY et al. have reported that in chronic myeloid leukemia cells, *METTL3* modulates the expression of *NEAT1* through m<sup>6</sup>A modification, and that upregulation of miR-766-5p inhibits *NEAT1* function(45). Interestingly, *CDKN1A* is a miR-766-

5p target gene, and *CDKN1A* knockdown can reverse the impacts of *NEAT1*, suggesting that the *METTL3*/*NEAT1*/miR-766-5p/*CDKN1A* axis is important in chronic myeloid leukemia. These outcomes highlight the importance of *METTL3* in regulating *CDKN1A* expression. Our study found that the knockdown of *METTL3* in the HT-22 cells led to an increased expression of *CDKN1A*, a reduction in m<sup>6</sup>A modification, and enhanced mRNA stability. These results suggest that *METTL3* regulates hippocampal neuronal cell function by modulating *CDKN1A* expression, likely through its influence on m<sup>6</sup>A methylation and mRNA stability. Although we have not yet experimentally mapped the precise m<sup>6</sup>A sites on *CDKN1A*, there is evidence suggesting that this transcript may carry functional m<sup>6</sup>A modifications. For instance, *POPI* has been shown to bind the CDS region of *CDKN1A* mRNA and promote its degradation in an m<sup>6</sup>A-dependent manner at position 497, a site recognized by YTHDF2(46). In addition, *CDKN1A* has been reported as a potential downstream target of *METTL3* and may undergo m<sup>6</sup>A-mediated regulation in certain biological contexts(43, 47). These findings imply that *METTL3*-recognizable m<sup>6</sup>A motifs are likely present on *CDKN1A*. In future work, m<sup>6</sup>A mapping assays would be performed to validate specific m<sup>6</sup>A sites on *CDKN1A* and to clarify how *METTL3*-dependent methylation regulates its stability and function in hippocampal neurons.

Cyclin Dependent Kinase Inhibitor 1A (*CDKN1A*) is a vital cell cycle regulator, primarily functioning as an inhibitor of cyclin-dependent kinases(48). It is essential for preserving cell cycle arrest in reaction to DNA damage, thereby promoting cell survival or initiating apoptosis when necessary(49). Recent studies demonstrate that *CDKN1A* is essential in cognitive impairment and neuronal dysfunction, as its overexpression can lead to neuronal cell cycle re-entry, causing neurodegeneration(50). In Kumon H et al., haloperidol exposure during pregnancy resulted in the upregulation of apoptotic genes, including *CDKN1A* and *APAF1*, in the hippocampus of offspring, highlighting the potential impact of antipsychotics on neuronal development(51). Similarly, Luyckx E et al. have reported that the loss of neuroglobin (Ngb) expression in neural stem cells (NSCs) led to increased proliferation, as indicated by the downregulation of *CDKN1A* and

upregulation of *CDK6*, both of which promote cell cycle progression(52). These findings suggest that alterations in *CDKN1A* expression can influence key cellular pathways, affecting neuronal and stem cell behavior.

Hippocampal damage or degeneration has been closely linked to various cognitive impairments and neurodegenerative diseases(53, 54). Several studies have suggested that the hippocampus possesses a degree of self-repair capacity, especially following mild damage(55). For instance, Konakanchi S et al. have reported that CSD led to impairments in spatial memory, increased anxiety-like behaviors, and a reduction in dendritic branching of CA3 hippocampal neurons in rats(56). However, after 21 days of sleep recovery, improvements in memory, anxiety, and oxidative stress were observed. Similarly, Xie G et al. have found that sleep deprivation resulted in cognitive decline and hippocampal neuronal damage, with low-dose caffeine improving cognitive function while high-dose caffeine exacerbated cognitive damage(57). In the current investigation, we analyzed the levels of *METTL3*, *CDKN1A*, and apoptosis-related proteins in the hippocampus of CSD-treated and *METTL3*-overexpressing rats. Our outcomes demonstrated that *METTL3* overexpression alleviated the reduction of *METTL3* caused by CSD, suppressed *CDKN1A*, and decreased the apoptosis-related proteins expression. Furthermore, MWM tests and histological analysis of hippocampal CA3 neurons indicated that *METTL3* overexpression could restore cognitive function and neuronal integrity in CSD rats. Additionally, in hippocampal neurons, silencing *METTL3* was confirmed to induce apoptosis through the upregulation of *CDKN1A*. These outcomes imply that *METTL3* provides protection in the hippocampus, potentially via modulation of *CDKN1A* expression and apoptotic pathways, highlighting its therapeutic potential in mitigating cognitive decline and neurodegeneration.

Several limitations of this study should be acknowledged. First, only male rats were included, which may limit the generalizability of our findings to females. Second, the sample size was relatively modest, potentially reducing statistical power and the robustness of certain analyses,

such as WGCNA. Third, HT-22 cells are an immortalized hippocampal neuronal line and may not fully recapitulate the physiological properties of primary neurons, particularly regarding synaptic protein expression. Key functional results therefore require validation in primary neuronal cultures. Fourth, our *in vitro* experiments cannot entirely replicate the complex *in vivo* conditions of chronic sleep deprivation. Finally, while we demonstrate that *METTL3* regulates *CDKN1A* stability via m<sup>6</sup>A, the precise m<sup>6</sup>A modification motif has not yet been identified, and the role of m<sup>6</sup>A readers such as YTHDF2 remains to be explored.

To address these limitations and guide future research, studies should validate our findings in female animals and clinical samples to assess generalizability and translational relevance. Key functional results should be confirmed in primary neuronal cultures, and the roles of m<sup>6</sup>A motifs and readers such as YTHDF2 should be investigated. Additionally, exploring targeted drug interventions and evaluating their efficacy in preclinical trials will provide practical strategies for mitigating CSD-induced cognitive impairment. By acknowledging these limitations and outlining these directions, we aim to provide a balanced interpretation of our findings and inform subsequent studies.

## 5. Conclusion

This study suggests that *METTL3* critically regulates cognitive function and neuronal survival under CSD conditions. Downregulation of *METTL3* in CSD-induced model appears to promote cognitive deficits and neuronal apoptosis by modulating key target *CDKN1A* via m<sup>6</sup>A-dependent mechanisms. Notably, restoring *METTL3* expression is associated with alleviates hippocampal damage and improves cognitive performance, underscoring its therapeutic potential. These findings identify the *METTL3*-m<sup>6</sup>A-*CDKN1A* axis as a molecular driver of CSD-related pathophysiology.

## Author Contributions

Conception and design of the research: Fei Xing, Xiao-Shan Shi and Jian-Jun Yang

Acquisition of data: Fei Xing, Xiao-Shan Shi and Min Jia

Analysis and interpretation of data: Fei Xing, Han-Wen Gu, Pan-Miao Liu and Lei Lei

Statistical analysis: Xiao-Shan Shi, Xing-Ming Wang and Mu-Huo Ji

Drafting the manuscript: Fei Xing and Xiao-Shan Shi

Revision of manuscript for important intellectual content: Jian-Jun Yang

#### **Consent for publication**

Not applicable.

#### **Data availability statement**

The datasets used and/or analyzed during the current study are available from the corresponding author upon reasonable request.

#### **Conflict of interest disclosure**

The authors have no conflicts of interest to declare.

#### **Funding**

This study was supported by grants from Medical Science and Technology Research Project of Henan Province (No. SBGJ202403023), the National Natural Science Foundation of China (No. 82001187), the National Natural Science Foundation of China (No. U23A20421), and the Scientific Research and Innovation Team of The First Affiliated Hospital of Zhengzhou University (ZYCXTD2023012).

#### **Acknowledgments**

None.

#### **Permission to reproduce material from other sources**

Not application.

### Clinical trial registration

Not application.

### References

1. Gibson K, Kartsounis L, Kopelman M. Cognitive impairment and performance. Understanding doctors' performance: CRC Press; 2023. p. 48-60.
2. Newbury CR, Crowley R, Rastle K, Tamminen J. Sleep deprivation and memory: Meta-analytic reviews of studies on sleep deprivation before and after learning. *Psychological bulletin*. 2021;147(11):1215.
3. Kreutzmann J, Havekes R, Abel T, Meerlo P. Sleep deprivation and hippocampal vulnerability: changes in neuronal plasticity, neurogenesis and cognitive function. *Neuroscience*. 2015;309:173-90.
4. Xiao X, Rui Y, Jin Y, Chen M. Relationship of sleep disorder with neurodegenerative and psychiatric diseases: an updated review. *Neurochemical Research*. 2024;49(3):568-82.
5. Ochai J, Umana U, Musa S, Oladele S. Chronic sleep deprivation induces spatial memory impairment, chromatolysis, and histoarchitectural changes in the CA3 region of the hippocampus. *Journal of Experimental and Clinical Anatomy*. 2024;21(2):252-61.
6. Watson JF, Vargas-Barroso V, Morse-Mora RJ, Navas-Olive A, Tavakoli MR, Danzl JG, et al. Human hippocampal CA3 uses specific functional connectivity rules for efficient associative memory. *Cell*. 2025;188(2):501-14. e18.
7. Albadawi EA. Structural and functional changes in the hippocampus induced by environmental exposures. *Neurosciences Journal*. 2025;30(1):5-19.
8. Wen YL, Guo F, Gu Tt, Zeng Yp, Cao X. Transcriptomic Regulation by Astrocytic m6A Methylation in the mPFC. *Genes to Cells*. 2025;30(2):e70003.
9. Chen H, Guo F, Zhao Y, Liu W, Chen B, Wang C, et al. Effects of m6A methylation of MAT2A mRNA regulated by METTL16 on learning and memory, hippocampal synaptic plasticity and A $\beta$ 1–42 in 5 $\times$  FAD mice. *Frontiers in Aging Neuroscience*. 2025;17:1572976.
10. Xia W, Liu Y, Lu J, Cheung H-H, Meng Q, Huang B. RNA methylation in neurodevelopment and related diseases: RNA methylation in neurodevelopment and related diseases. *Acta Biochimica et Biophysica Sinica*. 2024;56(12):1723.
11. Yan L, Wei Ja, Yang F, Wang M, Wang S, Cheng T, et al. Physical exercise prevented stress - induced anxiety via improving brain RNA methylation. *Advanced Science*. 2022;9(24):2105731.
12. Zhang D, Gou Z, Qu Y, Su X. Mechanistic insights into vascular biology via methyltransferase-like 3-driven N6-adenosine methylation of RNA. *Frontiers in Cell and Developmental Biology*. 2025;12:1482753.
13. Xu P, Ge R. Roles and drug development of METTL3 (methyltransferase-like 3) in anti-tumor therapy. *European journal of medicinal chemistry*. 2022;230:114118.
14. Su X, Qu Y, Mu D. The regulatory network of METTL3 in the nervous system: diagnostic biomarkers and

- therapeutic targets. *Biomolecules*. 2023;13(4):664.
15. Niu J, Wang B, Wang T, Zhou T. Mechanism of METTL3 - mediated m6A modification in depression - induced cognitive deficits. *American Journal of Medical Genetics Part B: Neuropsychiatric Genetics*. 2022;189(3-4):86-99.
  16. Li Y, Xue J, Ma Y, Ye K, Zhao X, Ge F, et al. The complex roles of m6A modifications in neural stem cell proliferation, differentiation, and self-renewal and implications for memory and neurodegenerative diseases. *Neural Regeneration Research*. 2025;20(6):1582-98.
  17. Chen H, Xing H, Zhong C, Lin X, Chen R, Luo N, et al. METTL3 confers protection against mitochondrial dysfunction and cognitive impairment in an Alzheimer disease mouse model by upregulating Mfn2 via N6-methyladenosine modification. *Journal of Neuropathology & Experimental Neurology*. 2024;83(7):606-14.
  18. Zhao F, Xu Y, Gao S, Qin L, Austria Q, Siedlak SL, et al. METTL3-dependent RNA m 6 A dysregulation contributes to neurodegeneration in Alzheimer's disease through aberrant cell cycle events. *Molecular neurodegeneration*. 2021;16:1-25.
  19. Wang C-X, Cui G-S, Liu X, Xu K, Wang M, Zhang X-X, et al. METTL3-mediated m6A modification is required for cerebellar development. *PLoS biology*. 2018;16(6):e2004880.
  20. Arumugam T, Ghazi T, Chuturgoon AA. Fumonisins B1 alters global m6A RNA methylation and epigenetically regulates Keap1-Nrf2 signaling in human hepatoma (HepG2) cells. *Archives of Toxicology*. 2021;95(4):1367-78.
  21. Li Q, Li X, Tang H, Jiang B, Dou Y, Gorospe M, et al. NSUN2 - mediated m5C methylation and METTL3/METTL14 - mediated m6A methylation cooperatively enhance p21 translation. *Journal of cellular biochemistry*. 2017;118(9):2587-98.
  22. Leenaars CH, Dematteis M, Joosten RN, Eggels L, Sandberg H, Schirris M, et al. A new automated method for rat sleep deprivation with minimal confounding effects on corticosterone and locomotor activity. *Journal of neuroscience methods*. 2011;196(1):107-17.
  23. Chen J, Wei J, Ying X, Yang F, Zhao Y, Pu J. Establishing a Device for Sleep Deprivation in Mice. *Journal of visualized experiments : JoVE*. 2023(199).
  24. Luo Y-W, Xu Y, Cao W-Y, Zhong X-L, Duan J, Wang X-Q, et al. Insulin-like growth factor 2 mitigates depressive behavior in a rat model of chronic stress. *Neuropharmacology*. 2015;89:318-24.
  25. Tian H, Ding N, Guo M, Wang S, Wang Z, Liu H, et al. Analysis of learning and memory ability in an Alzheimer's disease mouse model using the Morris water maze. *JoVE (Journal of Visualized Experiments)*. 2019(152):e60055.
  26. Cao Y, Yang Y, Wu H, Lu Y, Wu S, Liu L, et al. Stem-leaf saponins from Panax notoginseng counteract aberrant autophagy and apoptosis in hippocampal neurons of mice with cognitive impairment induced by sleep deprivation. *Journal of ginseng research*. 2020;44(3):442-52.
  27. Rao X, Huang X, Zhou Z, Lin X. An improvement of the  $2^{\Delta\Delta CT}$  method for quantitative real-time polymerase chain reaction data analysis. *Biostatistics, bioinformatics and biomathematics*. 2013;3(3):71.
  28. Wang M-K, Gao C-C, Yang Y-G. Emerging roles of RNA methylation in development. *Accounts of Chemical Research*. 2023;56(23):3417-27.
  29. Abdivalievna AN. Features of cognitive disorders. *Innovative Society: Problems, Analysis and Development Prospects (Spain)*. 2022:101-5.
  30. Csipo T, Lipecz A, Owens C, Mukli P, Perry JW, Tarantini S, et al. Sleep deprivation impairs cognitive performance, alters task-associated cerebral blood flow and decreases cortical neurovascular coupling-related hemodynamic responses. *Scientific reports*. 2021;11(1):20994.
  31. Tang H, Li K, Dou X, Zhao Y, Huang C, Shu F. The neuroprotective effect of osthole against chronic sleep

- deprivation (CSD)-induced memory impairment in rats. *Life Sciences*. 2020;263:118524.
32. Wang X, Wang Z, Cao J, Dong Y, Chen Y. Gut microbiota-derived metabolites mediate the neuroprotective effect of melatonin in cognitive impairment induced by sleep deprivation. *Microbiome*. 2023;11(1):17.
33. Diao L-T, Xie S-J, Lei H, Qiu X-S, Huang M-C, Tao S, et al. METTL3 regulates skeletal muscle specific miRNAs at both transcriptional and post-transcriptional levels. *Biochemical and Biophysical Research Communications*. 2021;552:52-8.
34. Catlin JP, Schaner Tooley CE. Exploring potential developmental origins of common neurodegenerative disorders. *Biochemical Society Transactions*. 2024;BST20230422.
35. Zhang N, Ding C, Zuo Y, Peng Y, Zuo L. N6-methyladenosine and neurological diseases. *Molecular neurobiology*. 2022;59(3):1925-37.
36. Lu W, Huang T, Wang X-R, Zhou J-H, Yuan H-Z, Yang Y, et al. Next-generation sequencing: a follow-up of 36,913 singleton pregnancies with noninvasive prenatal testing in central China. *Journal of Assisted Reproduction and Genetics*. 2020;37:3143-50.
37. He B, Wang J. METTL3 regulates hippocampal gene transcription via N6-methyladenosine methylation in sevoflurane-induced postoperative cognitive dysfunction mouse. *Aging (Albany NY)*. 2021;13(19):23108.
38. Ming Y, Deng Z, Tian X, Jia Y, Ning M, Cheng S. m6A methyltransferase METTL3 reduces hippocampal neuron apoptosis in a mouse model of autism through the MALAT1/SFRP2/wnt/β-catenin Axis. *Psychiatry Investigation*. 2022;19(10):771.
39. Tudor JC, Davis EJ, Peixoto L, Wimmer ME, van Tilborg E, Park AJ, et al. Sleep deprivation impairs memory by attenuating mTORC1-dependent protein synthesis. *Science signaling*. 2016;9(425):ra41.
40. Li Y, Zhang Y, Ji G, Shen Y, Zhao N, Liang Y, et al. Autophagy Triggered by Oxidative Stress Appears to Be Mediated by the AKT/mTOR Signaling Pathway in the Liver of Sleep-Deprived Rats. *Oxidative medicine and cellular longevity*. 2020;2020:6181630.
41. Cao Y, Li Q, Liu L, Wu H, Huang F, Wang C, et al. Modafinil protects hippocampal neurons by suppressing excessive autophagy and apoptosis in mice with sleep deprivation. *British journal of pharmacology*. 2019;176(9):1282-97.
42. Zhang Y, Feng Y, Lu Y, Ying Y, Wang D, Ying X, et al. Semen Ziziphi Spinosae affects circadian rhythm of the cAMP signaling pathway by BMAL1-clockophagy to improve sleep disorders in depression. *Phytomedicine : international journal of phytotherapy and phytopharmacology*. 2025;148:157483.
43. Ouyang D, Hong T, Fu M, Li Y, Zeng L, Chen Q, et al. METTL3 depletion contributes to tumour progression and drug resistance via N6 methyladenosine-dependent mechanism in HR+HER2-breast cancer. *Breast cancer research : BCR*. 2023;25(1):19.
44. Shi Y, Zheng C, Jin Y, Bao B, Wang D, Hou K, et al. Reduced Expression of METTL3 Promotes Metastasis of Triple-Negative Breast Cancer by m6A Methylation-Mediated COL3A1 Up-Regulation. *Frontiers in oncology*. 2020;10:1126.
45. Yao F-Y, Zhao C, Zhong F-M, Qin T-Y, Wen F, Li M-Y, et al. m (6) A modification of lncRNA NEAT1 regulates chronic myelocytic leukemia progression via miR-766-5p/CDKN1A axis. *Frontiers in oncology*. 2021;11:679634.
46. Zhang C, Wang S, Lu X, Zhong W, Tang Y, Huang W, et al. POP1 Facilitates Proliferation in Triple-Negative Breast Cancer via m6A-Dependent Degradation of CDKN1A mRNA. *Research (Washington, DC)*. 2024;7:0472.
47. Li S, Zhou H, Liang Y, Yang Q, Zhang J, Shen W, et al. Integrated analysis of transcriptome-wide m(6)A methylation in a Cd-induced kidney injury rat model. *Ecotoxicology and environmental safety*. 2023;256:114903.
48. D'costa M, Bothe A, Das S, Kumar SU, Gnanasambandan R, Doss CGP. CDK regulators—Cell cycle progression or

- apoptosis—Scenarios in normal cells and cancerous cells. *Advances in Protein Chemistry and Structural Biology*. 2023;135:125-77.
49. Manousakis E, Miralles CM, Esquerda MG, Wright RH. CDKN1A/p21 in Breast Cancer: Part of the Problem, or Part of the Solution? *International Journal of Molecular Sciences*. 2023;24(24):17488.
  50. Porterfield V, Khan SS, Foff EP, Koseoglu MM, Blanco IK, Jayaraman S, et al. A three-dimensional dementia model reveals spontaneous cell cycle re-entry and a senescence-associated secretory phenotype. *Neurobiology of aging*. 2020;90:125-34.
  51. Kumon H, Yoshino Y, Ozaki T, Funahashi Y, Mori H, Ueno M, et al. Gestational exposure to haloperidol changes Cdkn1a and Apaf1 mRNA expressions in mouse hippocampus. *Brain Research Bulletin*. 2023;199:110662.
  52. Luyckx E, Van Leuven W, Andre D, Quarta A, Reekmans K, Fransen E, et al. Loss of neuroglobin expression alters Cdkn1a/Cdk6-expression resulting in increased proliferation of neural stem cells. *Stem Cells and Development*. 2018;27(6):378-90.
  53. Terreros-Roncal J, Moreno-Jiménez EP, Flor-García M, Rodríguez-Moreno CB, Trinchero MF, Cafini F, et al. Impact of neurodegenerative diseases on human adult hippocampal neurogenesis. *Science*. 2021;374(6571):1106-13.
  54. Rao YL, Ganaraja B, Murlimanju B, Joy T, Krishnamurthy A, Agrawal A. Hippocampus and its involvement in Alzheimer's disease: a review. *3 Biotech*. 2022;12(2):55.
  55. Wan Q, Sun K, Liu T, Qin P. Memristive Neural Network Circuit of Negative Emotion Inhibition With Self - Repair and Memory. *International Journal of Circuit Theory and Applications*. 2024.
  56. Konakanchi S, Raavi V, MI HK, Shankar V. Effect of chronic sleep deprivation and sleep recovery on hippocampal CA3 neurons, spatial memory and anxiety-like behavior in rats. *Neurobiology of Learning and Memory*. 2022;187:107559.
  57. Xie G, Huang X, Li H, Wang P, Huang P. Caffeine-related effects on cognitive performance: Roles of apoptosis in rat hippocampus following sleep deprivation. *Biochemical and Biophysical Research Communications*. 2021;534:632-8.

## Figure legends

### **Figure 1. Differential gene expression and functional analysis in the hippocampal CA3 region of CSD rats.**

(A) Volcano plot showing the differential expression of genes in m<sup>6</sup>A RNA-Seq data. Each point represents a gene, with the x-axis indicating the log<sub>2</sub> fold change and the y-axis indicating the -log<sub>10</sub> p-value. Genes that are significantly upregulated (orange) or downregulated (blue) are labeled, with *METTL3* (highlighted in red) showing significant expression differences. (B) Heatmap of the DEGs between control (n=3) and CSD groups (n=3). The color scale represents the normalized expression levels, with orange indicating higher expression and purple indicating

lower expression. Samples are clustered by group, with the control samples in green and the CSD samples in red. (C) GO enrichment analysis of DEGs. The x-axis represents the gene ratio, and the y-axis shows the top enriched biological processes. The size of the circles corresponds to the number of genes involved, while the color intensity represents the significance (-log<sub>10</sub> p-value). (D) KEGG pathway analysis showing the top enriched pathways associated with the DEGs. The x-axis represents the gene ratio, and the y-axis lists the pathways. Circle size represents the number of DEGs involved in each pathway, while color intensity indicates the significance of each pathway (-log<sub>10</sub> p-value). (E) Boxplot showing the expression levels of *METTL3* in the CSD and control groups. The y-axis represents *METTL3* expression levels. \*P < 0.05 vs. Control group. CSD: Chronic sleep deprivation, DEGs: Differentially expressed genes, GO: Gene ontology, KEGG: Kyoto encyclopedia of genes and genomes.

**Figure 2. *METTL3* is downregulated in the hippocampal CA3 region in the CSD-induced cognitive impairment.**

(A) A schematic diagram illustrating the experimental timeline. Five-week-old male SD rats were subjected to a 21-day adaptation period, followed by 42 days of CSD induction. Afterward, MWM training was performed for 5 consecutive days, and testing was conducted on Day 6. (B-D) MWM behavioral tests. (B) Representative swimming path of the control and CSD groups in the MWM test (n=10). The red dot indicates the starting point, and the green dot represents the target location. (C) Frequency of crossing the platform (n=10). \*P < 0.05 vs. Control group. (D) Time spent in the target quadrant during the MWM test (n=10). \*P < 0.05 vs. Control group. (E) Relative mRNA expression levels of *METTL3* were significantly decreased in the CSD group compared to the control group, as determined by qRT-PCR (n=10). \*P < 0.05 vs. Control group. (F and G) WB analysis of *METTL3* protein levels in the CA3 region and quantification of relative protein expression levels (n=3). \*P < 0.05 vs. Control group. CSD: Chronic sleep deprivation, qRT-PCR: Quantitative real-time reverse transcription PCR, WB: Western blot, MWM: Morris water maze.

**Figure 3. METTL3 knockdown aggravates Rap-induced apoptosis in HT-22 cells.**

(A) qRT-PCR analysis showed that *METTL3* mRNA expression was significantly reduced after siRNA-mediated knockdown (si-*METTL3*-1 and si-*METTL3*-2) in HT-22 cells (n=3). \*P<0.05 vs. Control group. (B and C) WB and quantification confirmed decreased METTL3 protein expression following siRNA transfection (n=3). \*P < 0.05 vs. Control group. (D) CCK-8 analysis for the effect of different concentrations of rapamycin on cell viability (n=3). (E and F) Flow cytometric analysis of apoptosis in HT-22 cells treated with Rap and/or si-*METTL3* (n=3). Early and late apoptotic populations were defined based on Annexin V–PI quadrant gating: Q1 (PI<sup>+</sup>/Annexin V<sup>-</sup>): necrotic cells, Q2 (PI<sup>+</sup>/Annexin V<sup>+</sup>): late apoptotic cells, Q3 (PI<sup>-</sup>/Annexin V<sup>+</sup>): early apoptotic cells, Q4 (PI<sup>-</sup>/Annexin V<sup>-</sup>): viable cells. \*P < 0.05 vs. Control group; #P < 0.05 vs. Rap+si-NC group. (G-I) WB was used to detect the expression of apoptosis-related proteins in HT-22 cells before and after *METTL3* knockdown and Rap induction (n=3). \*P < 0.05 vs. Control group; #P < 0.05 vs. Rap+si-NC group. CSD: Chronic sleep deprivation, qRT-PCR: Quantitative real-time reverse transcription PCR, WB: Western blot, CCK8: Cell Counting Kit-8, Rap: Rapamycin.

**Figure 4. WGCNA analysis of RNA-seq data of *METTL3*-knockdown in HT-22 neuronal cells.**

(A) Sample dendrogram with/without trait heatmap. The hierarchical clustering of samples based on gene expression shows clustering of siRNA and NC groups (n=3). The heatmap beneath the dendrogram shows the trait distribution for each sample. (B) Selection of the soft threshold power for WGCNA. The plot shows the relationship between the soft threshold power (x-axis) and the scale-free topology fit index (y-axis). (C) Cluster dendrogram of genes. The hierarchical clustering of genes is shown, with gene modules assigned different colors according to the dynamic tree cut method. The colors at the bottom represent the different modules identified in the network. (D) EigenGene adjacency heatmap. The heatmap displays the correlation between ME from different modules. Strong positive correlations (red) and weak or negative correlations (blue) are indicated. (E) Correlation heatmap of module and gene significance. (F and G) Scatter plots of module membership versus gene significance in the brown (F) and green (G) modules. WGCNA: Weighted

gene co-expression network analysis, ME: Module eigengenes.

**Figure 5. Differential gene expression and functional enrichment analysis in *METTL3* knockdown HT-22 cells.**

(A) Volcano plot depicting the differential gene expression between si-*METTL3*-1 group (n=3) and NC groups (n=3). Genes that are significantly upregulated (orange) or downregulated (purple) are highlighted. The x-axis represents the  $\log_2$  fold change, and the y-axis represents the  $-\log_{10} p$ -value. (B) Venn diagram showing the overlap between DEGs and the genes in the green and brown modules identified by WGCNA. (C) GO analysis of DEGs. The x-axis represents the gene ratio (proportion of DEGs annotated to each term), and the y-axis shows the terms. The size of the circles corresponds to the number of DEGs in each pathway, and the color intensity represents the significance of each pathway ( $-\log_{10} P$ -value). (D) KEGG pathway enrichment analysis of DEGs in the si-*METTL3* group. The x-axis represents the gene ratio, and the y-axis lists the top enriched pathways. The size of the circles indicates the number of DEGs involved in each pathway, and color intensity represents the significance ( $-\log_{10} P$ -value). (E) Boxplot showing the expression levels of selected DEGs in *METTL3* knockdown and NC groups. \*P < 0.05 or \*\*P < 0.01 or \*\*\*P < 0.001 vs. si-NC group. NC: Negative control, WGCNA: Weighted gene co-expression network analysis, GO: Gene ontology, KEGG: Kyoto encyclopedia of genes and genomes, DEGs: Differentially expressed genes.

**Figure 6. Effect of *METTL3* knockdown on *CDKN1A* expression, m<sup>6</sup>A modification, and RNA stability in HT-22 cells.**

(A-C) *CDKN1A* expression analysis after *METTL3* knockdown. qRT-PCR (A) and WB (B, C) were performed to assess the mRNA and protein levels of *CDKN1A* in HT-22 cells transfected with si-NC or si-*METTL3*-1 (n=3). \*P < 0.05 vs. si-NC group. (D) Relative m<sup>6</sup>A enrichment fold change in HT-22 cells transfected with si-NC or si-*METTL3*-1 (n=3). \*P < 0.05 vs. si-NC group. (E) *CDKN1A* mRNA stability after *METTL3* knockdown. Actinomycin D treatment was used to

measure the stability of *CDKN1A* mRNA in HT-22 cells transfected with si-NC or si-*METTL3*-1 (n=3). \*P < 0.05 vs. si-NC group. qRT-PCR: Quantitative real-time polymerase chain reaction, WB: Western blot.

**Figure 7. METTL3 overexpression modulates CDKN1A expression and apoptotic pathways in the hippocampus of CSD rats.**

(A-C) WB analysis of METTL3 and CDKN1A protein expression in the hippocampus of CSD rats following *METTL3* overexpression. (A) Representative WB for METTL3 and CDKN1A proteins (n=3). (B) Quantification of METTL3 expression (n=3). (C) Quantification of CDKN1A expression (n=3). \*P < 0.05 vs. Control group; #P < 0.05 vs. CSD+vector group. (D-F) Expression of apoptosis-related proteins in the hippocampus of CSD rats. (D) Representative WB for Bax, Caspase-3 and cleaved Caspase-3 (n=3). (E) Quantification of Bax expression (n=3). (F) Quantification of cleaved Caspase-3 expression (n=3). \*P < 0.05 vs. Control group. (G-I) Effect of *METTL3* overexpression on apoptosis-related protein expression in the hippocampus of CSD rats. (G) Representative WB for Bax, Caspase-3 and cleaved Caspase-3 (n=3). (H) Quantification of Bax expression (n=3). (I) Quantification of cleaved Caspase-3 expression (n=3). \*P < 0.05 vs. Control group; #P < 0.05 vs. CSD+vector group. WB: Western blot, CSD: Chronic sleep deprivation.

**Figure 8. Impact of CSD and METTL3 overexpression on cognitive behavioral and hippocampal neuronal damage in rats.**

(A) MWM trajectory analysis showing the paths taken by rats from the control (n=10), CSD + vector (n=10), and CSD + over-METTL3 groups (n=10). The red circle indicates the target area, and the tracks demonstrate differences in spatial navigation. (B) Quantification of platform crossings (n=10). \*P<0.05 vs. Control group. #P<0.05 vs. CSD+vector group. (C) Time spent in the target quadrant (n=10). \*P < 0.05 vs. Control group; #P < 0.05 vs. CSD+vector group. (D) Representative H&E staining images of hippocampal tissue to evaluate neuronal damage in the

CA3 region (n=3). Scale bars: 500  $\mu\text{m}$  (top), 100  $\mu\text{m}$  (bottom). (E-F) Representative Nissl staining images of hippocampal neurons in the CA3 region to assess structural damage and distribution. (E) Representative images of Nissl-stained neurons in the CA3 region (n=3). The black box indicates the region of interest (ROI) used for quantification. (F) Quantification of injured cells/total cells in the enlarged region (%) based on Nissl staining (n=3). Scale bars: 500  $\mu\text{m}$  (top), 100  $\mu\text{m}$  (bottom). \*P < 0.05 vs. Control group;  $^{\#}$ P < 0.05 vs. CSD+vector group. CSD: Chronic sleep deprivation, MWM: Morris water maze, H&E: hematoxylin and eosin.

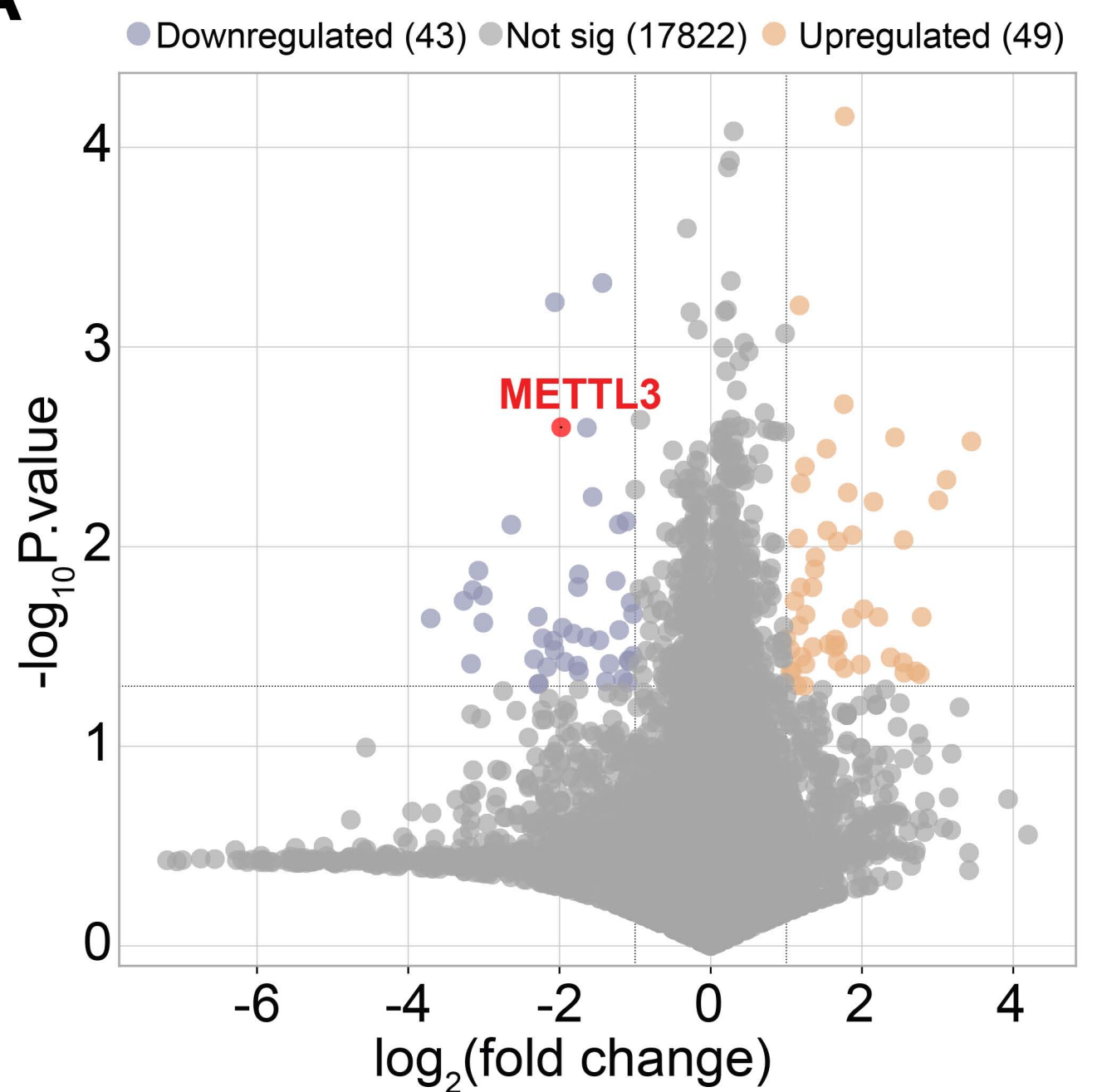
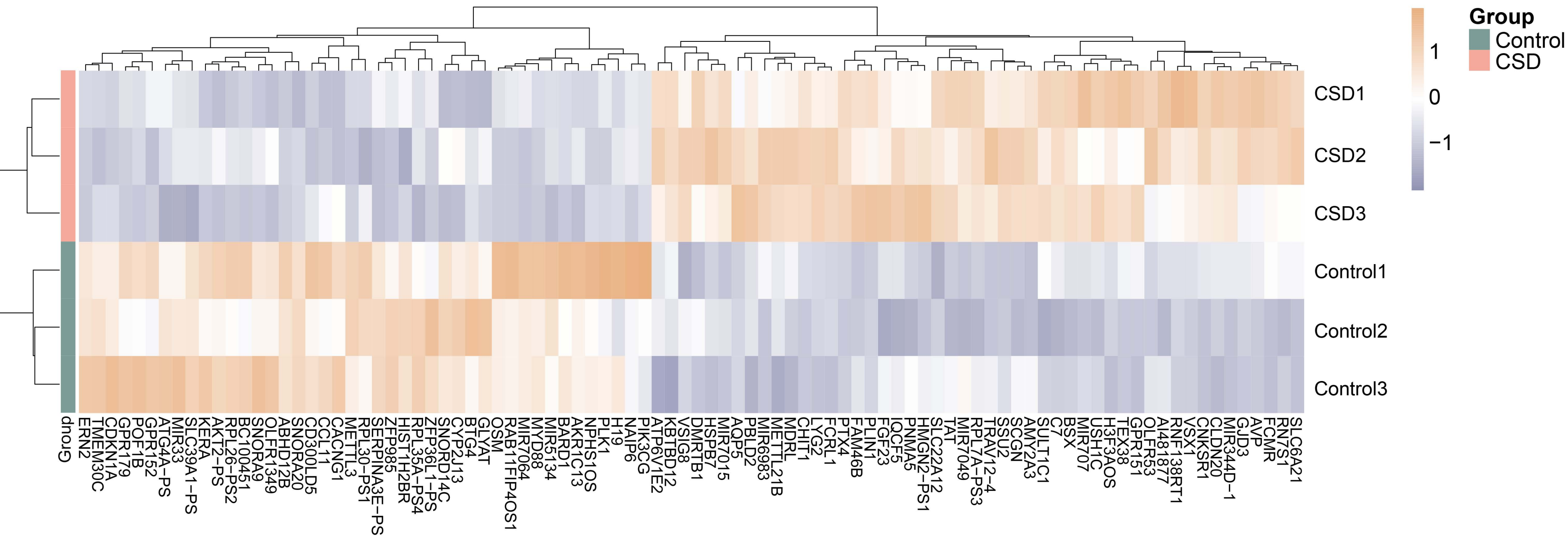
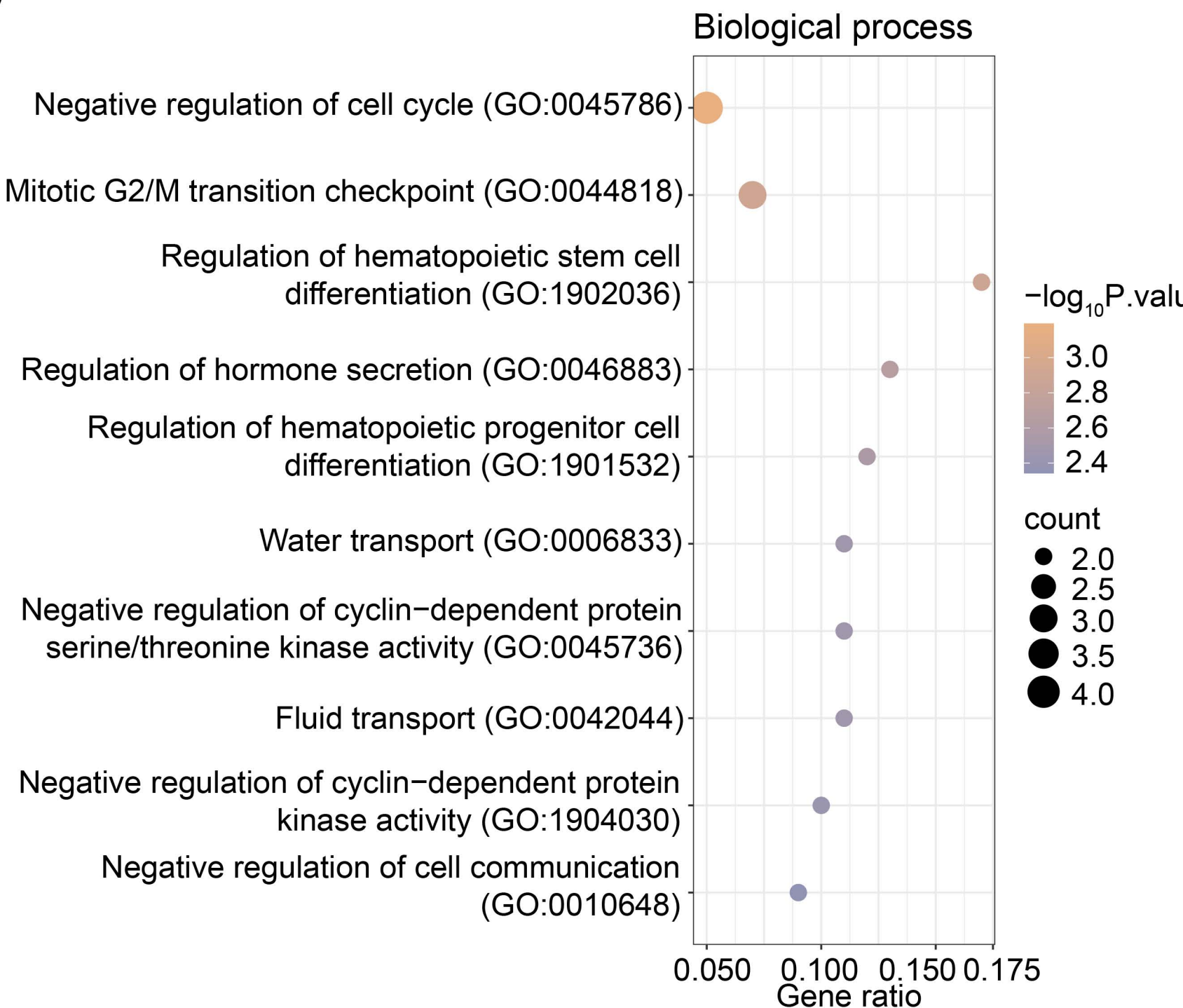
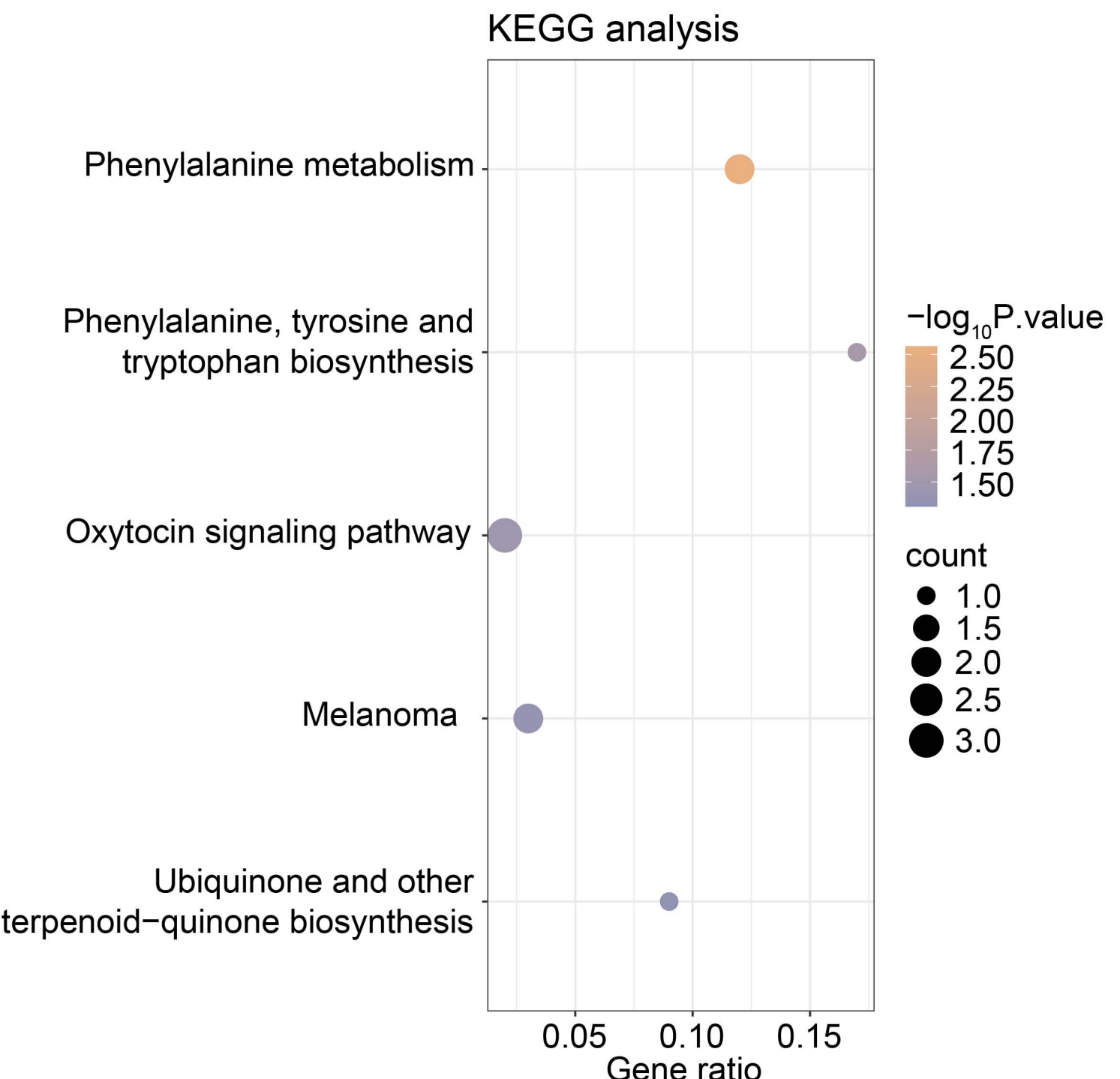
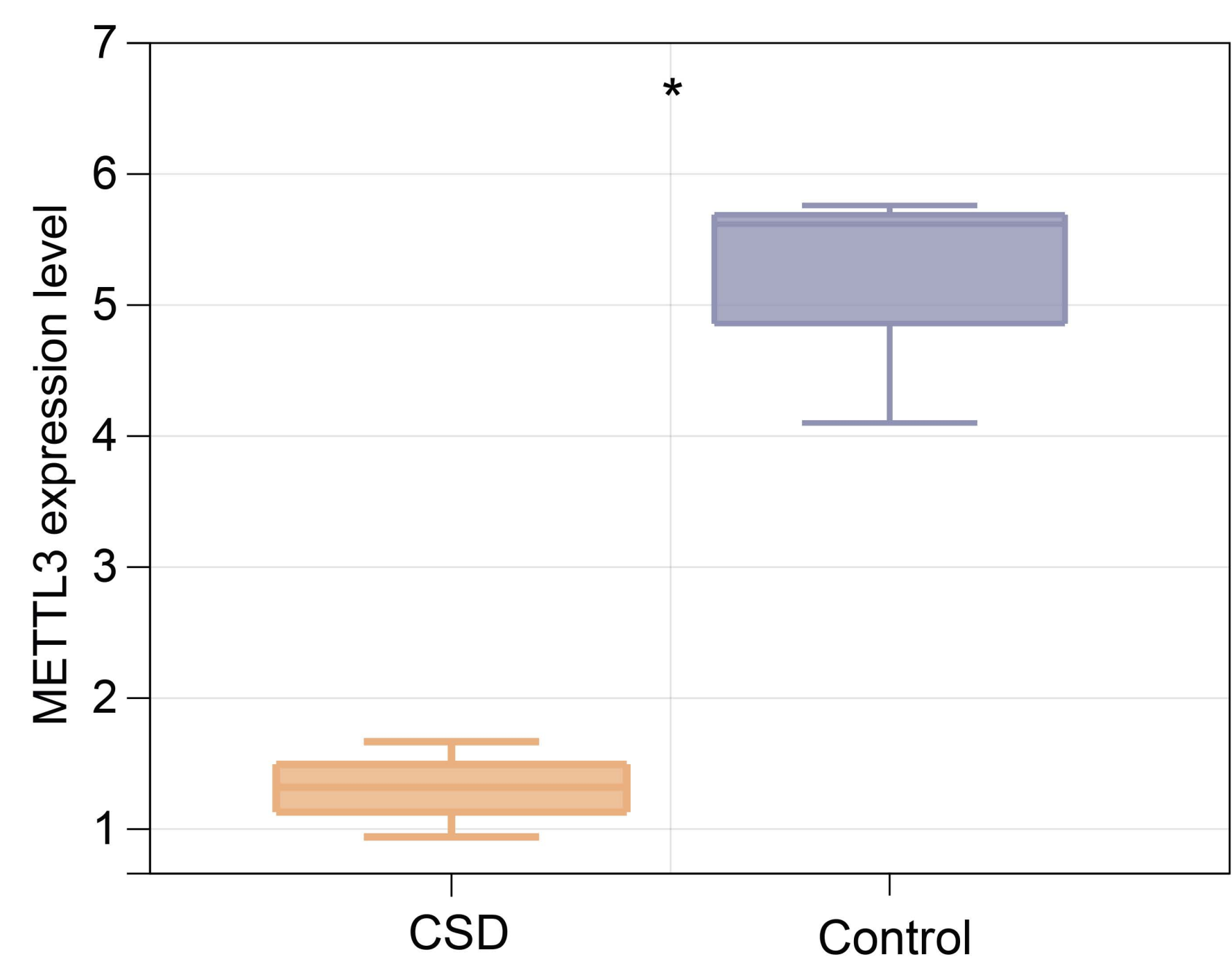
**Figure 9. METTL3 knockdown promotes neuronal apoptosis through the CDKN1A dependent pathway in HT-22 cells.**

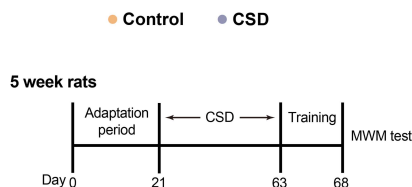
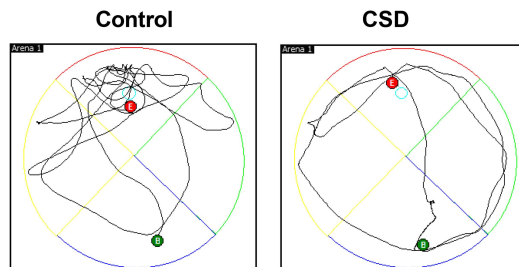
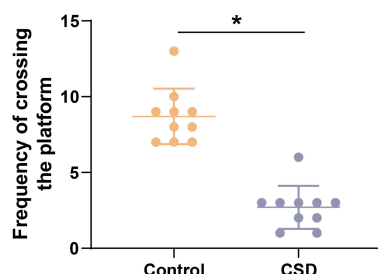
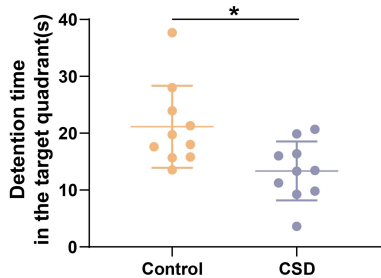
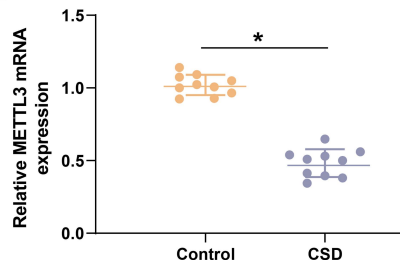
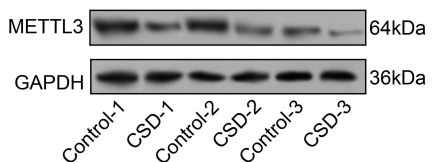
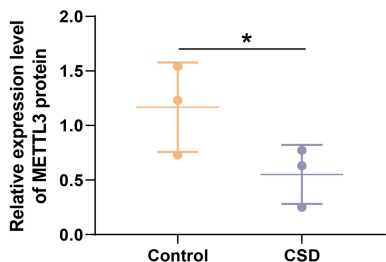
(A) Confirmation of *CDKN1A* overexpression in HT-22 cells via qRT-PCR (n=3). \*P < 0.05 vs. Oe-NC group. (B-C) Confirmation of *CDKN1A* overexpression in HT-22 cells by WB. (B) Representative WB images showing *CDKN1A* protein levels. (C) Quantification of *CDKN1A* protein expression (n=3). \*P < 0.05 vs. Oe-NC group. (D) qRT-PCR analysis of *CDKN1A* mRNA expression in HT-22 cells following *CDKN1A* overexpression and/or *METTL3* knockdown (n=3). \*P < 0.05 vs. Oe-NC group;  $^{\#}$ P < 0.05 vs. si-NC+over-*CDKN1A* group. (E-F) WB analysis of *CDKN1A* protein expression in HT-22 cells. (E) Representative WB images showing *CDKN1A* protein expression. (F) Quantification of *CDKN1A* protein expression in HT-22 cells under different treatment conditions (n=3). \*P < 0.05 vs. Oe-NC group;  $^{\#}$ P < 0.05 vs. si-NC+over-*CDKN1A* group. (G-H) Flow cytometry analysis of apoptosis in HT-22 cells following *CDKN1A* overexpression and/or *METTL3* knockdown. (G) Representative flow cytometry plots showing apoptosis levels. Early and late apoptotic populations were defined based on Annexin V-PI quadrant gating: Q1 (PI<sup>+</sup>/Annexin V<sup>-</sup>): necrotic cells, Q2 (PI<sup>+</sup>/Annexin V<sup>+</sup>): late apoptotic cells, Q3 (PI<sup>-</sup>/Annexin V<sup>+</sup>): early apoptotic cells, Q4 (PI<sup>-</sup>/Annexin V<sup>-</sup>): viable cells. (H) Quantification of apoptosis percentage (n=3). \*P < 0.05 vs. Oe-NC group;  $^{\#}$ P < 0.05 vs. si-NC+over-*CDKN1A* group. (I) Validation of *CDKN1A* knockdown efficiency in HT-22 cells via qRT-PCR (n=3). \*P < 0.05 vs. si-NC group. (J-K) Validation of *CDKN1A* knockdown efficiency in HT-22 cells by WB.

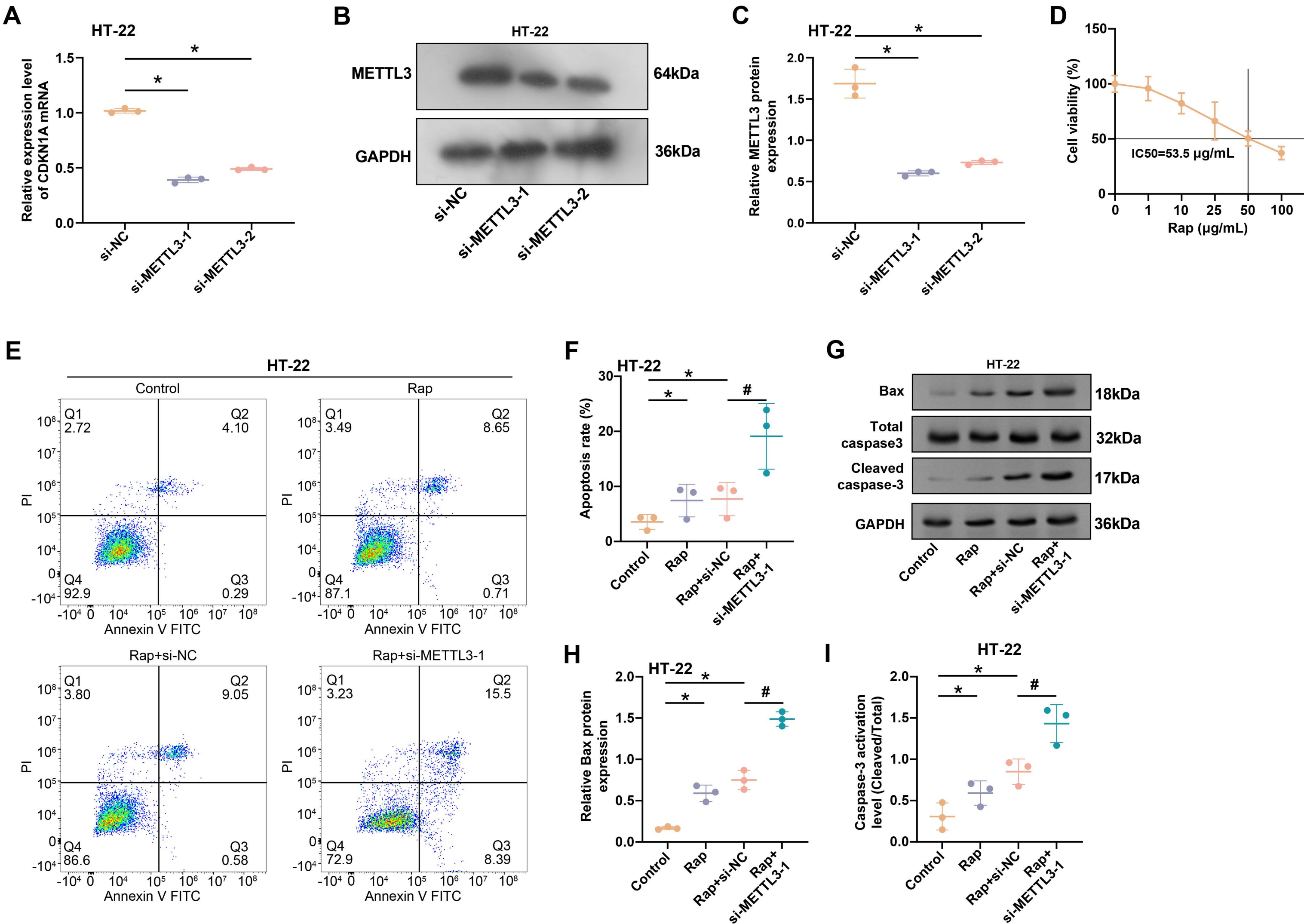
(J) Representative WB images showing *CDKN1A* protein levels. (K) Quantification of *CDKN1A* protein expression (n=3). \*P < 0.05 vs. si-NC group. (L) Analysis of *CDKN1A* mRNA expression in HT-22 cells following co-knockdown of *METTL3* and *CDKN1A* via qRT-PCR (n=3). \*P < 0.05 vs. si-NC group; <sup>#</sup>P < 0.05 vs. si-*METTL3*+si-NC group. (M–N) Analysis of *CDKN1A* protein expression in HT-22 cells following co-knockdown of *METTL3* and *CDKN1A* by WB. (M) Representative WB images showing *CDKN1A* protein levels. (N) Quantification of *CDKN1A* protein expression (n=3). \*P < 0.05 vs. si-NC group; <sup>#</sup>P < 0.05 vs. si-*METTL3*+si-NC group. (O–P) Effect of co-knockdown of *METTL3* and *CDKN1A* on cell apoptosis in HT-22 cells. (O) Representative flow cytometry plots showing apoptosis levels. Early and late apoptotic populations were defined based on Annexin V–PI quadrant gating: Q1 (PI<sup>+</sup>/Annexin V<sup>-</sup>): necrotic cells, Q2 (PI<sup>+</sup>/Annexin V<sup>+</sup>): late apoptotic cells, Q3 (PI<sup>-</sup>/Annexin V<sup>+</sup>): early apoptotic cells, Q4 (PI<sup>-</sup>/Annexin V<sup>-</sup>): viable cells. (P) Quantification of apoptosis percentage (n=3). \*P < 0.05 vs. si-NC group; <sup>#</sup>P < 0.05 vs. si-*METTL3*+si-NC group. WB: Western blot, qRT-PCR: quantitative reverse transcription PCR.

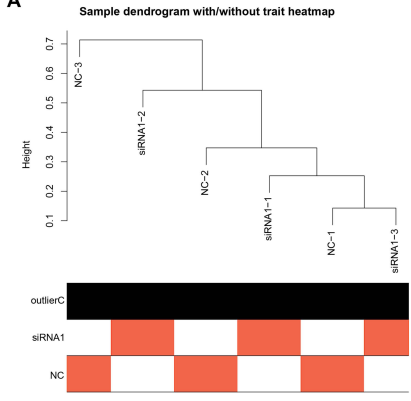
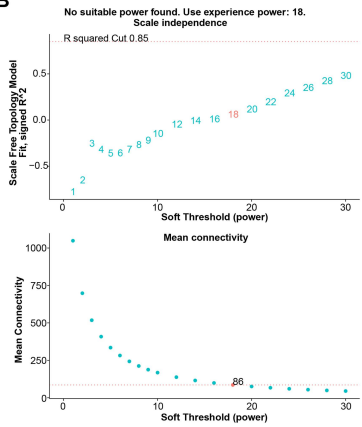
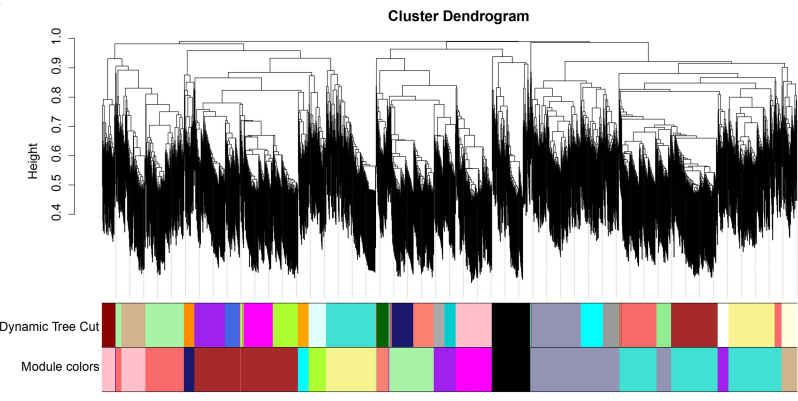
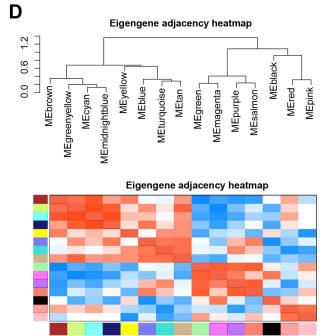
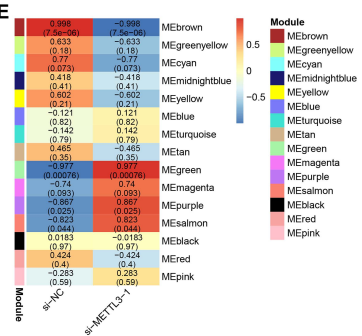
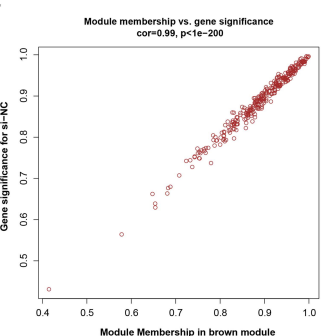
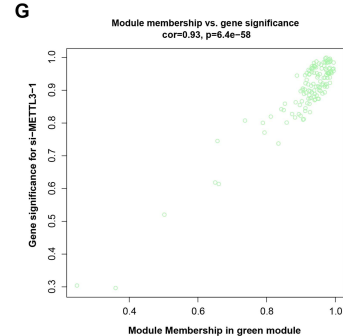
**Figure 10. Molecular mechanism of CSD-induced neuronal apoptosis and cognitive dysfunction.**

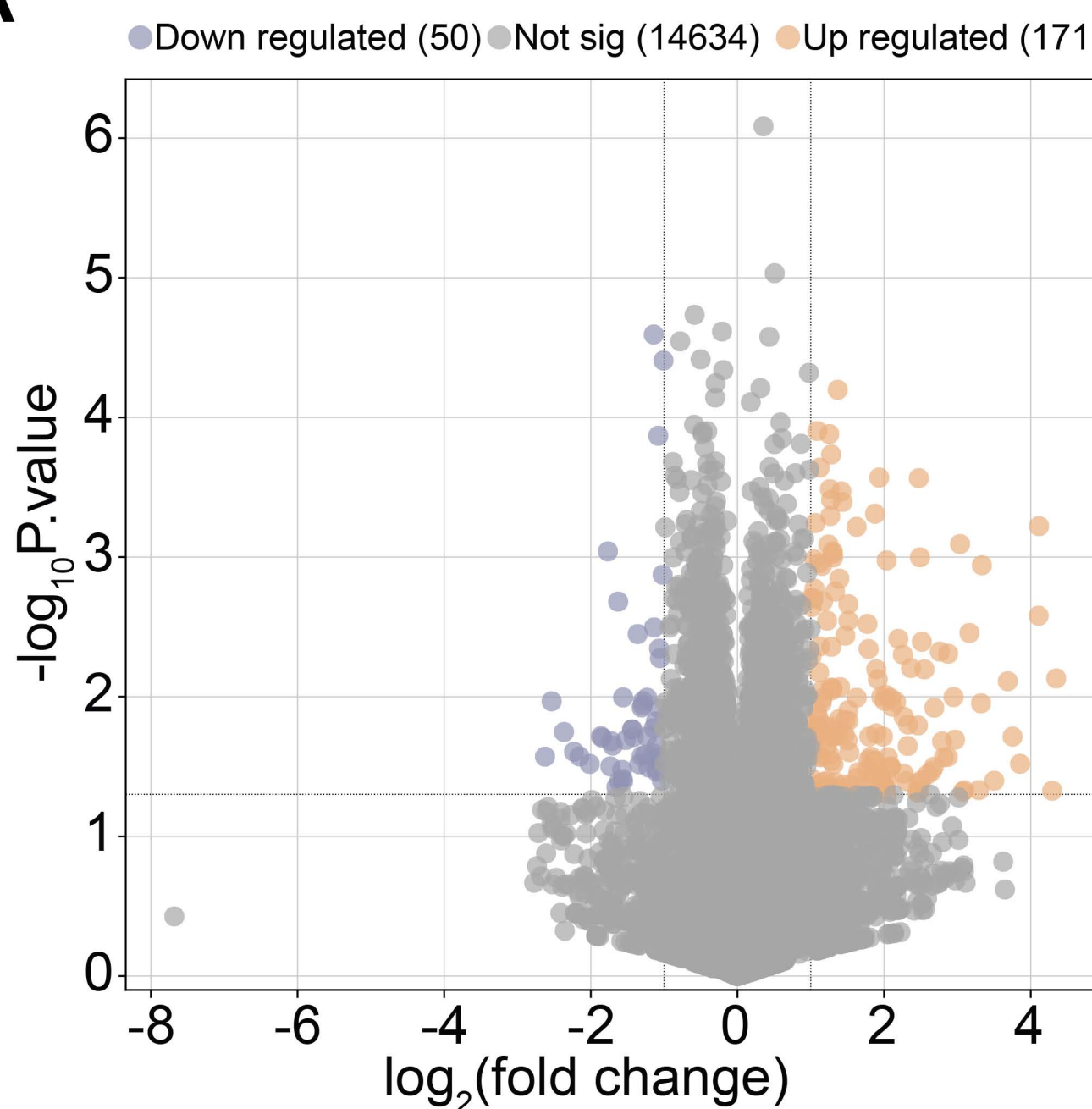
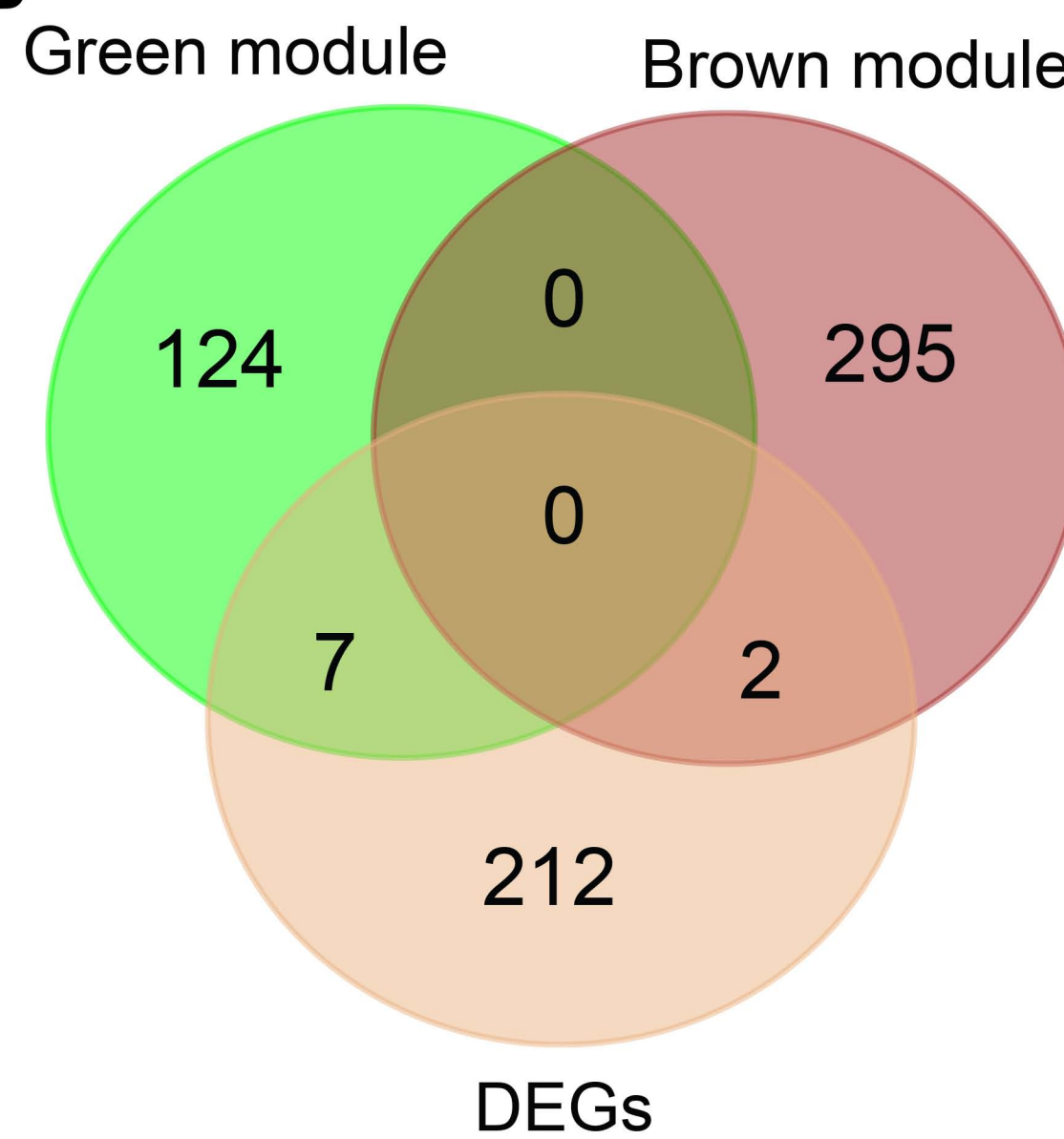
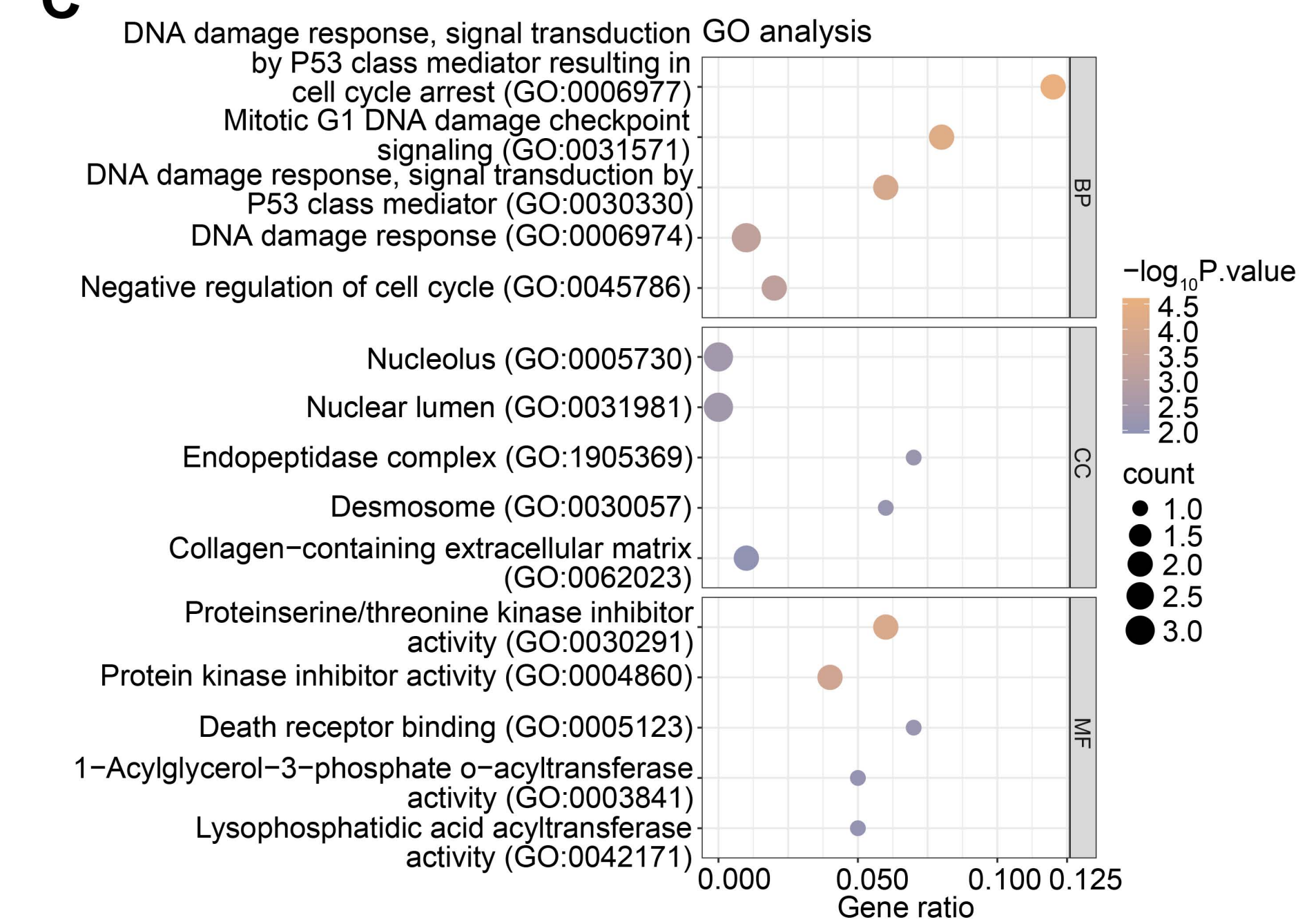
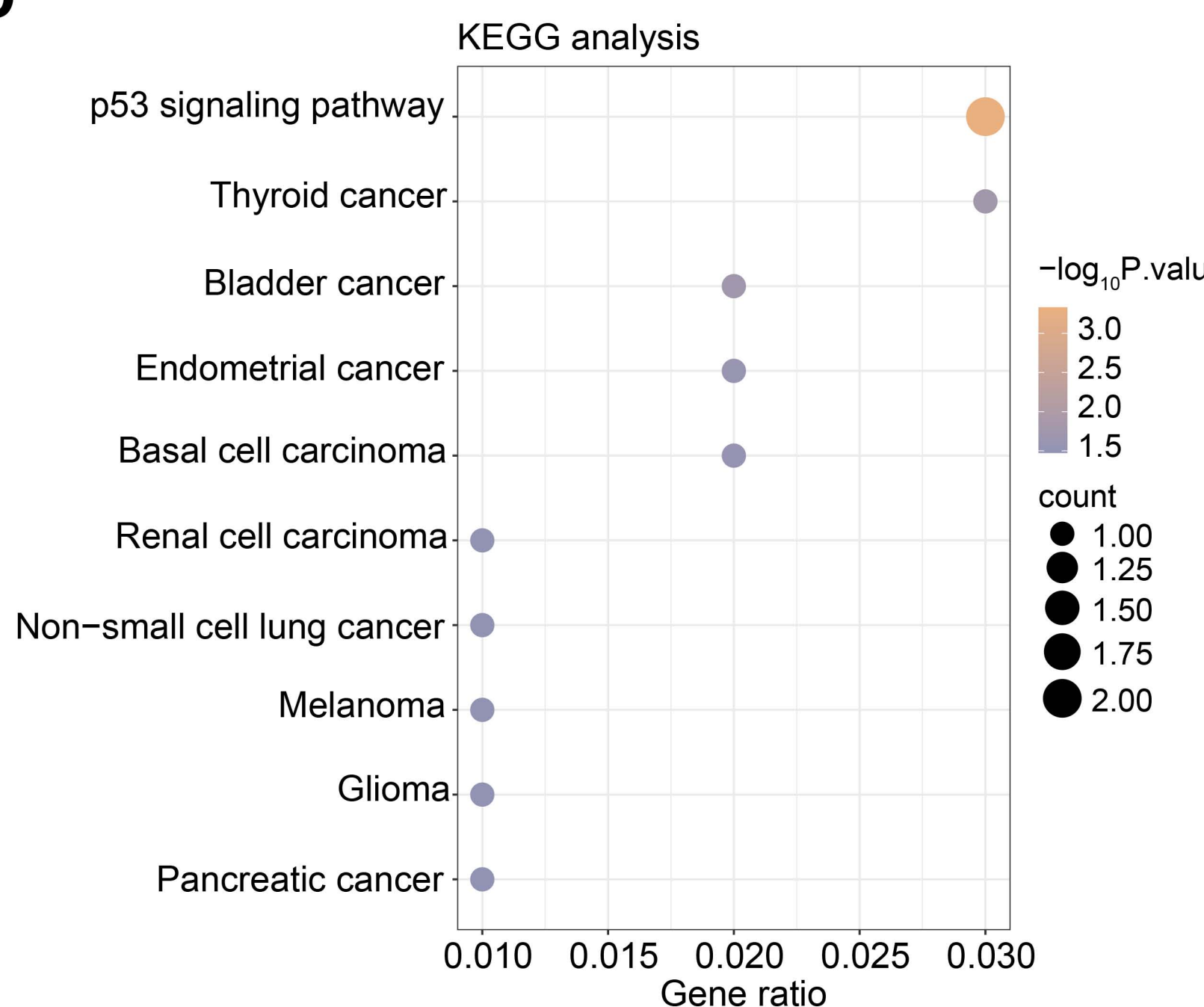
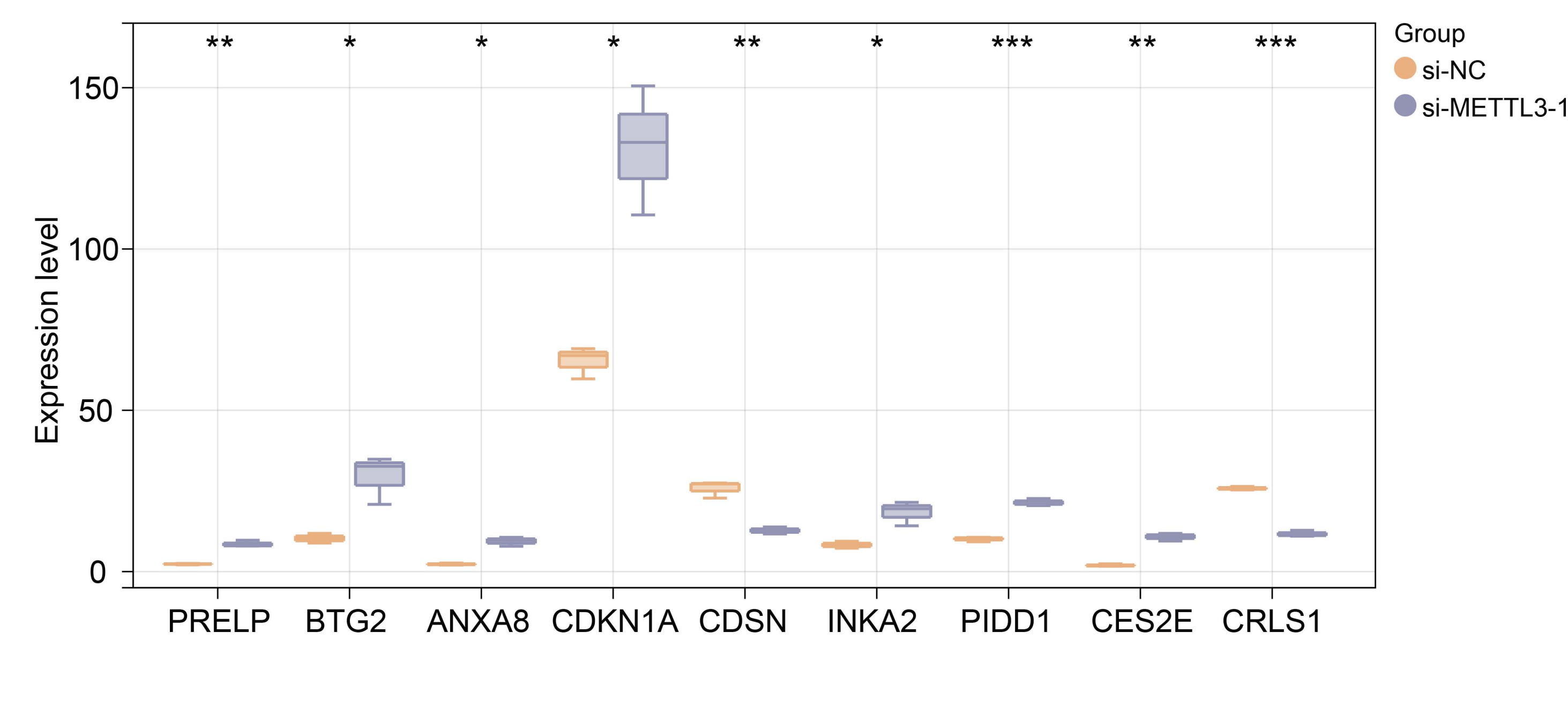
Schematic illustration of the proposed mechanism by which CSD induces neuronal apoptosis and cognitive dysfunction via the *METTL3*-m<sup>6</sup>A-*CDKN1A* axis. CSD: Chronic sleep deprivation, m<sup>6</sup>A: N6-methyladenosine, *METTL3*: methyltransferase-like 3, *CDKN1A*: cyclin-dependent kinase inhibitor 1A, Bax: Bcl-2-associated X protein, Caspase-3: cysteine aspartate-3.

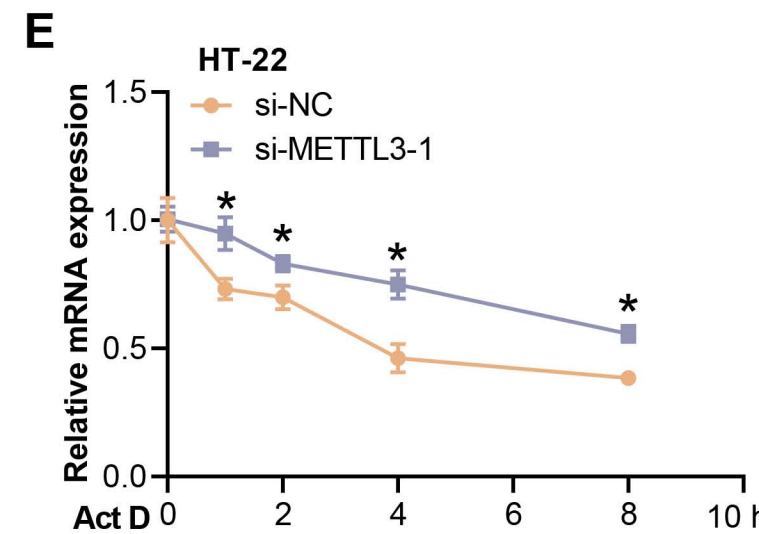
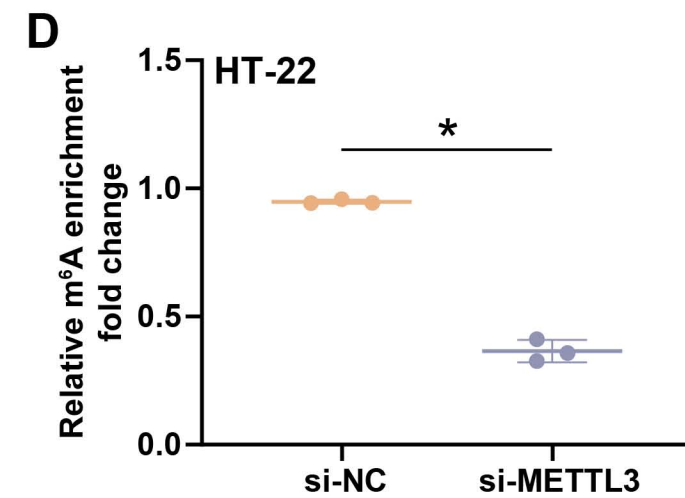
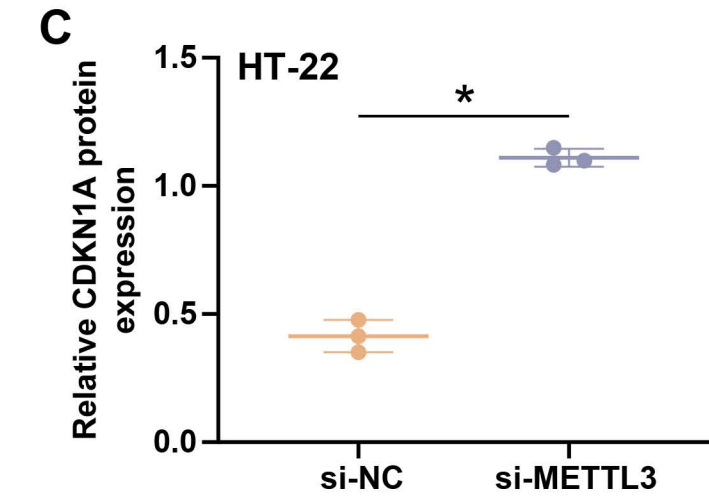
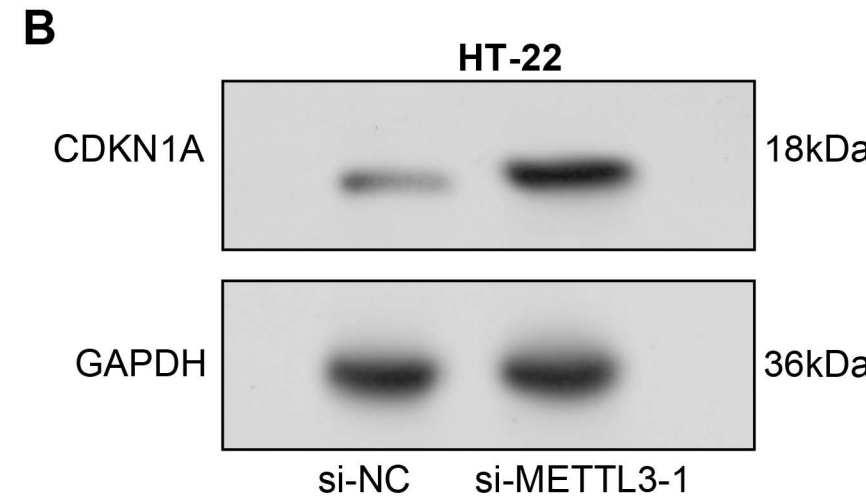
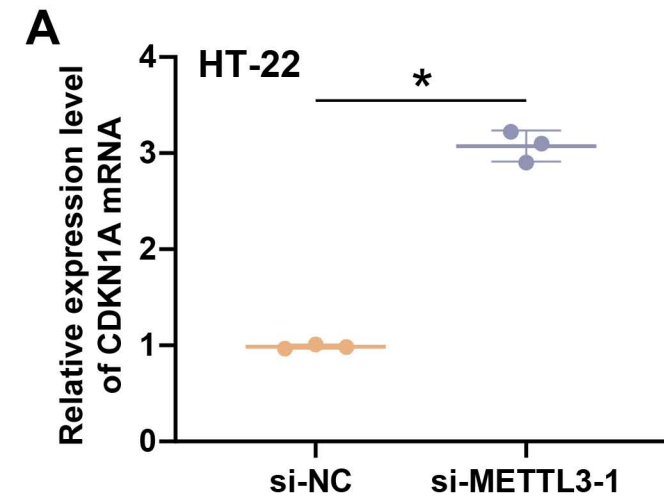
**A****B****C****D****E**

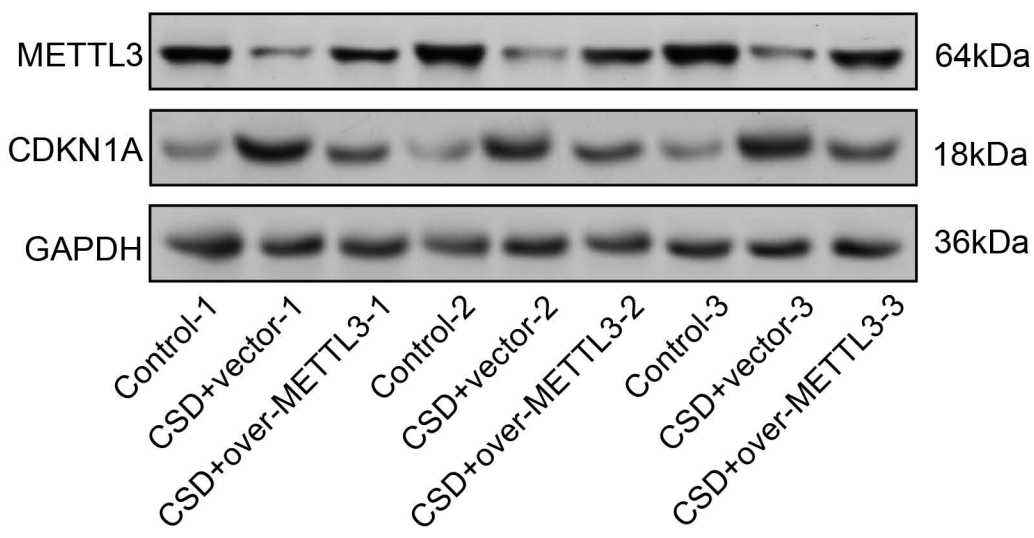
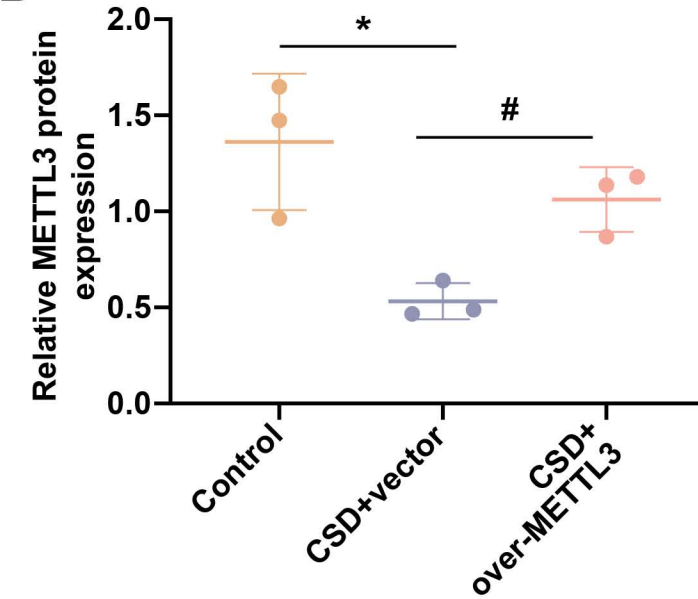
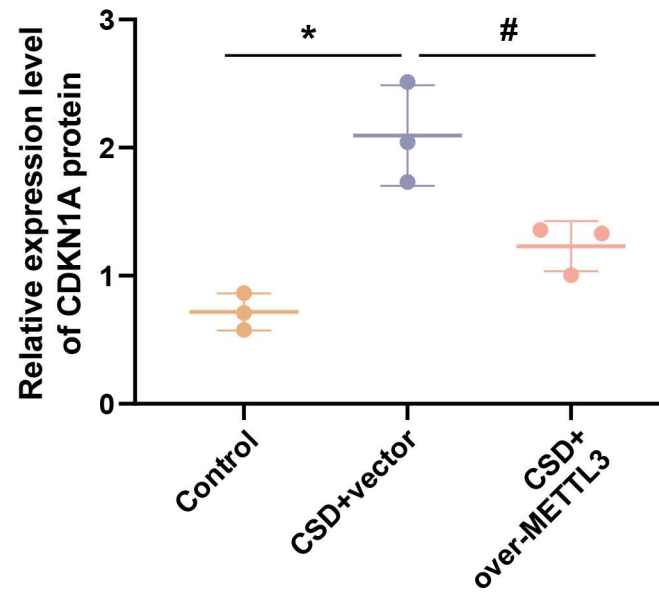
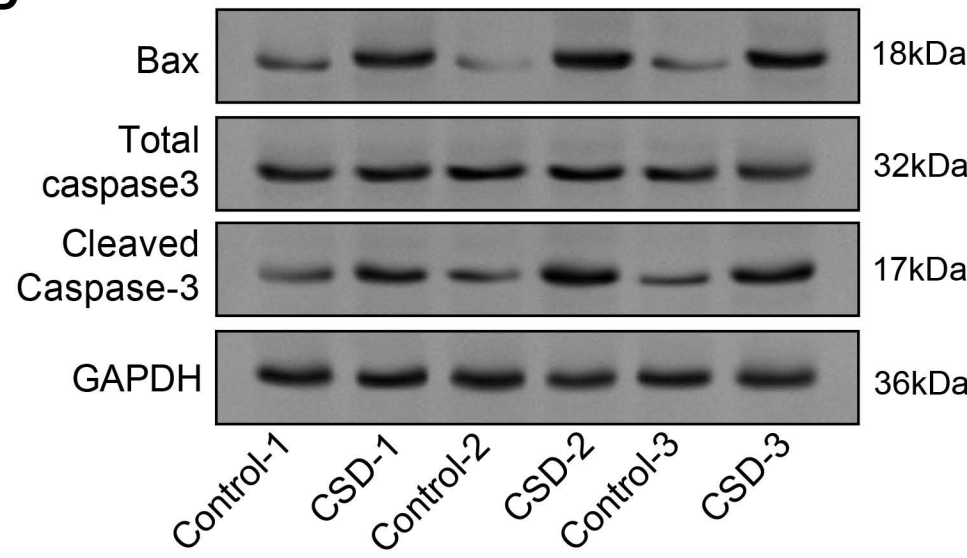
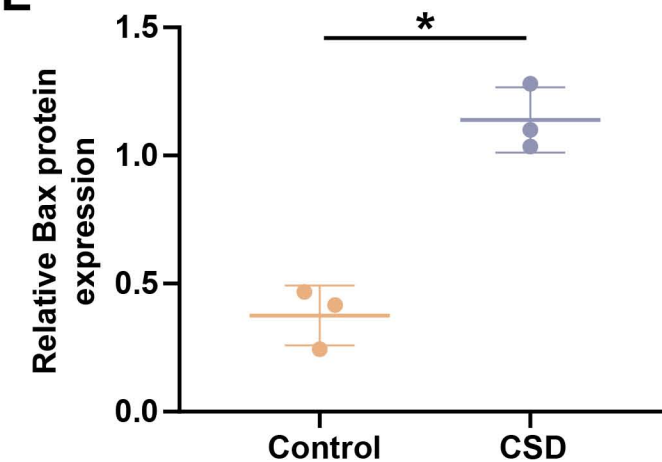
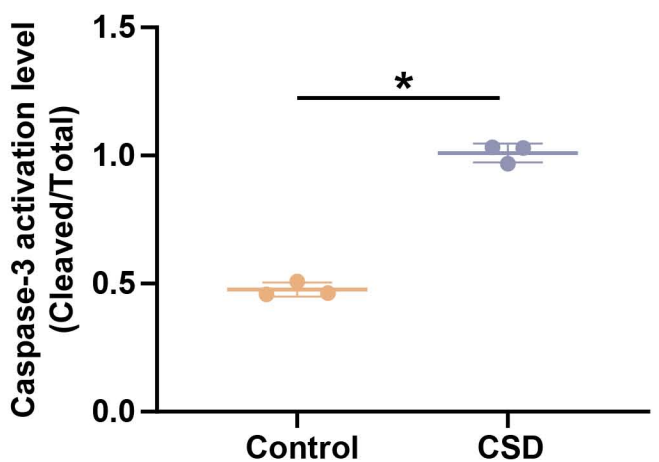
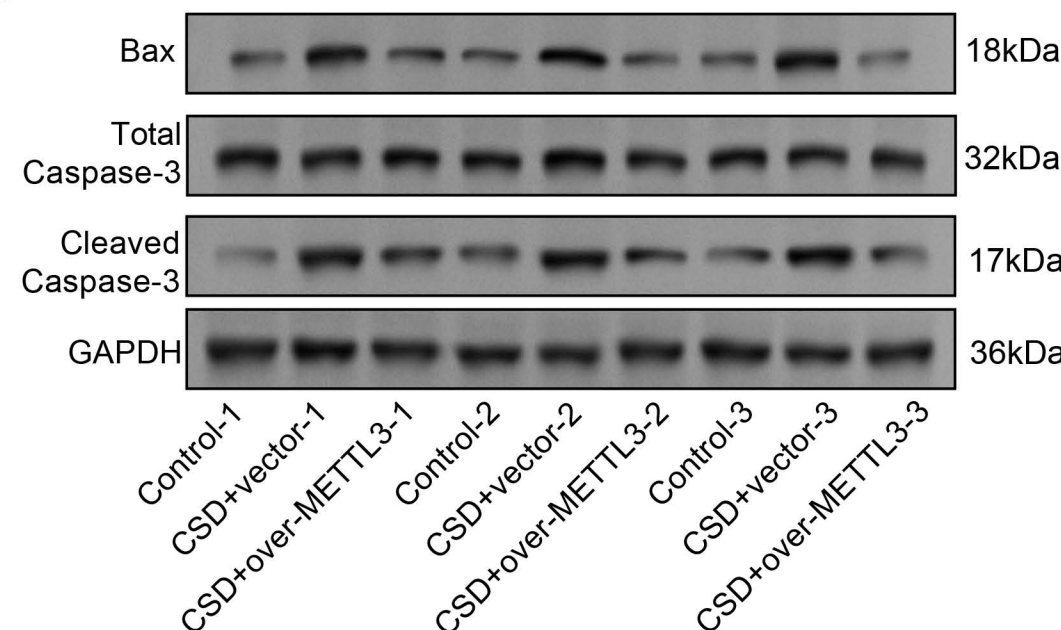
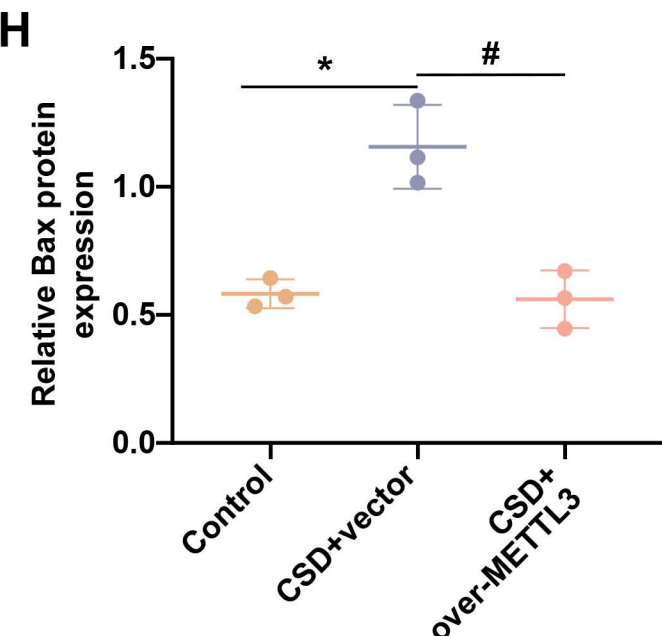
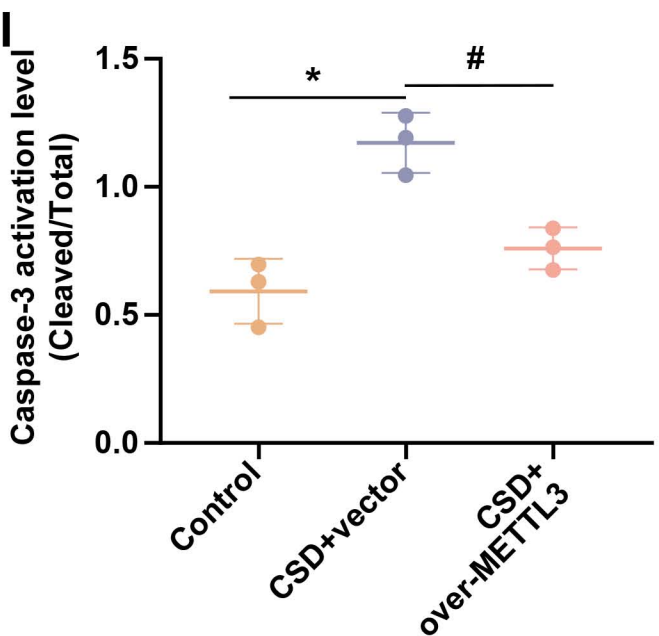
**A****B****C****D****E****F****G**

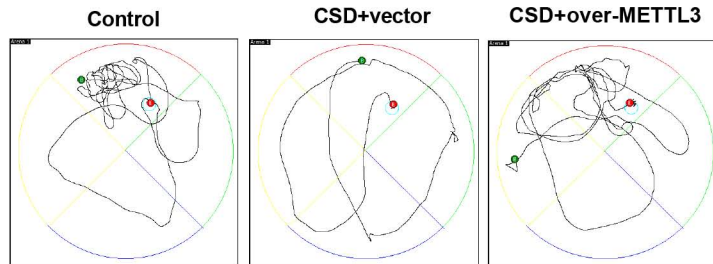
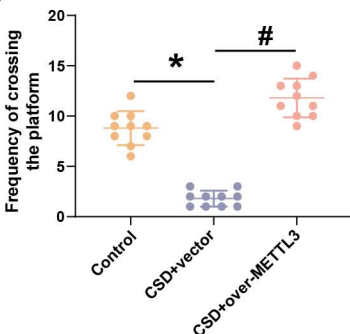
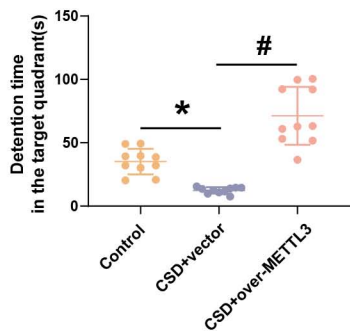
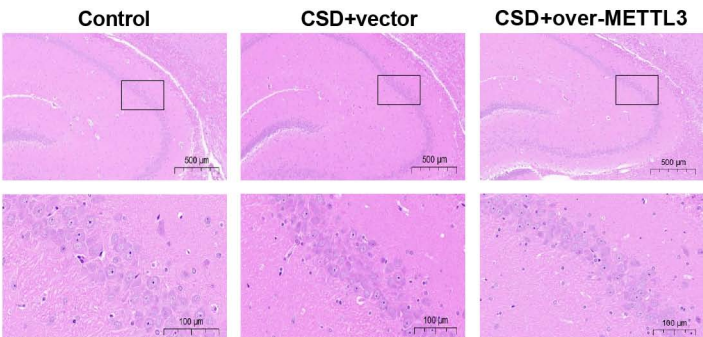
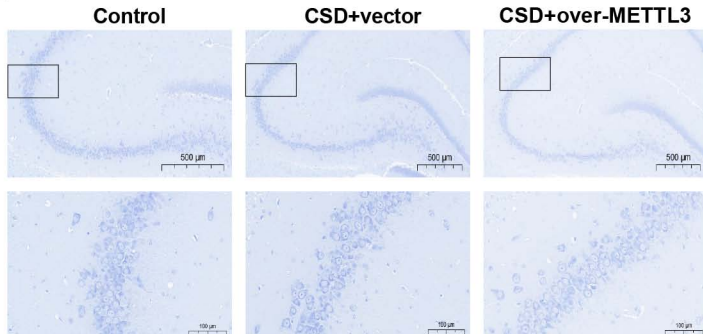
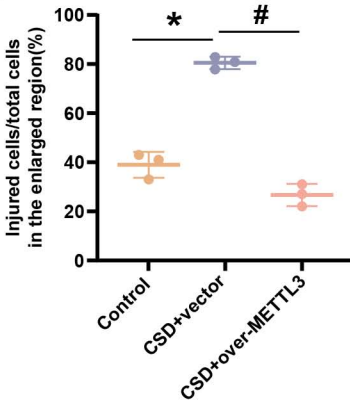


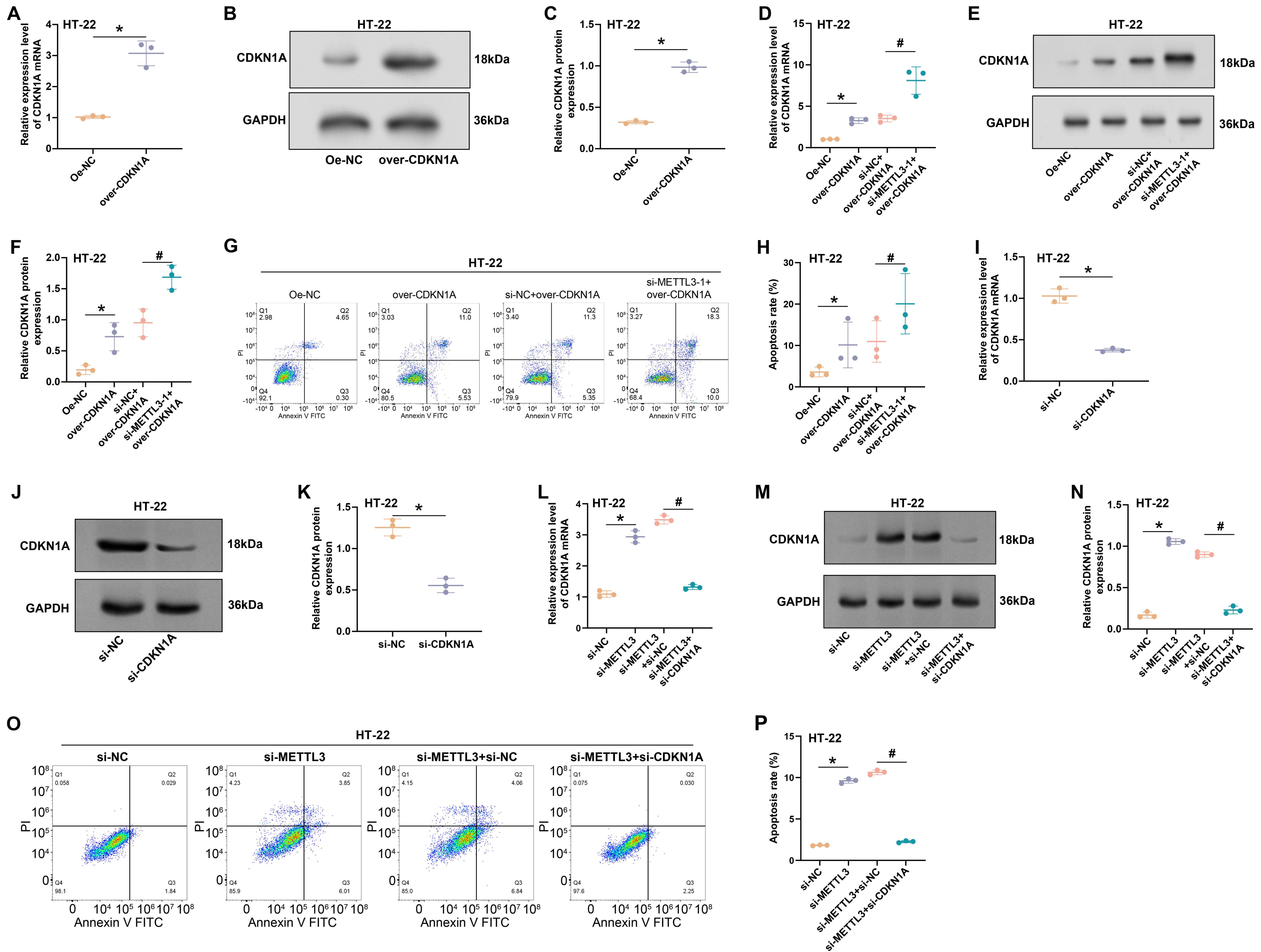
**A****B****C****D****E****F****G**

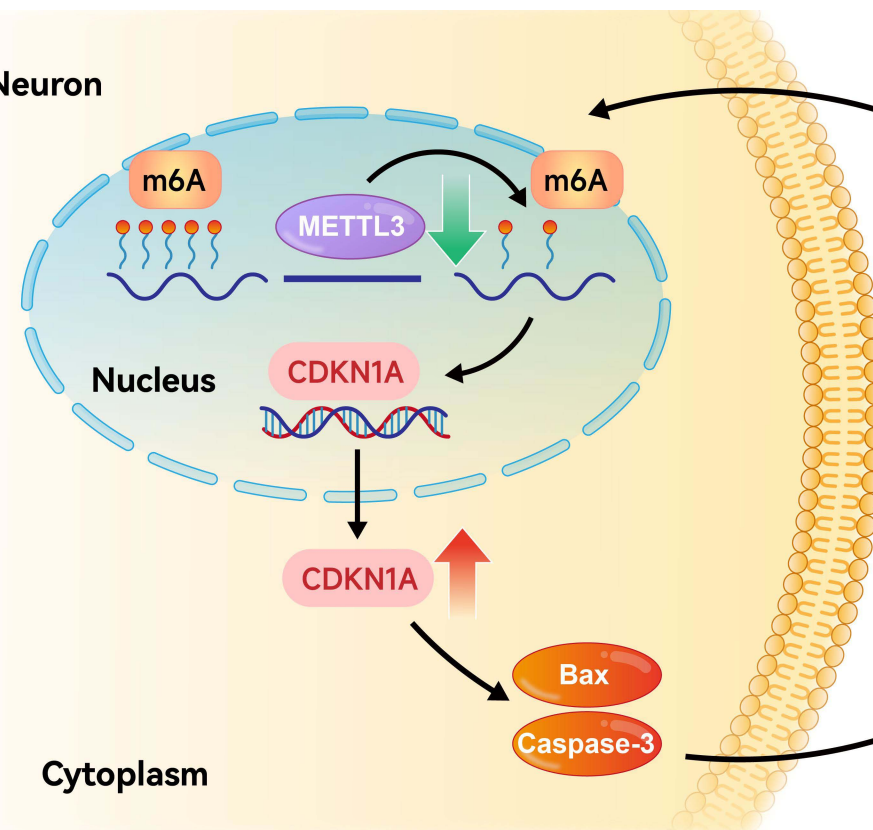
**A****B****C****D****E**



**A****B****C****D****E****F****G****H****I**

**A****B****C****D****E****F**

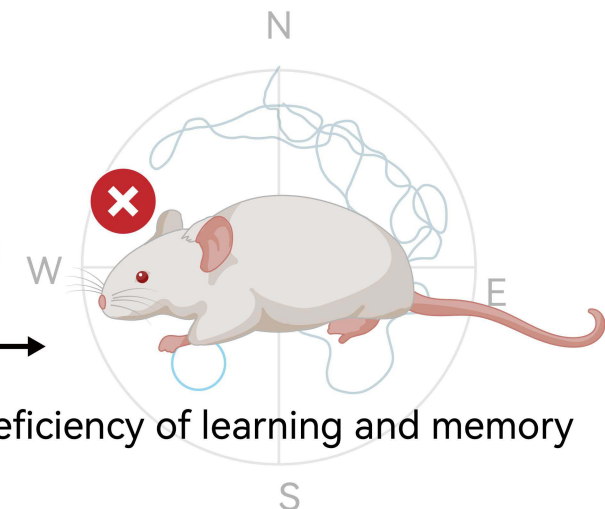


**Neuron**

Chronic sleep deprivation



Deficiency of learning and memory



Apoptosis